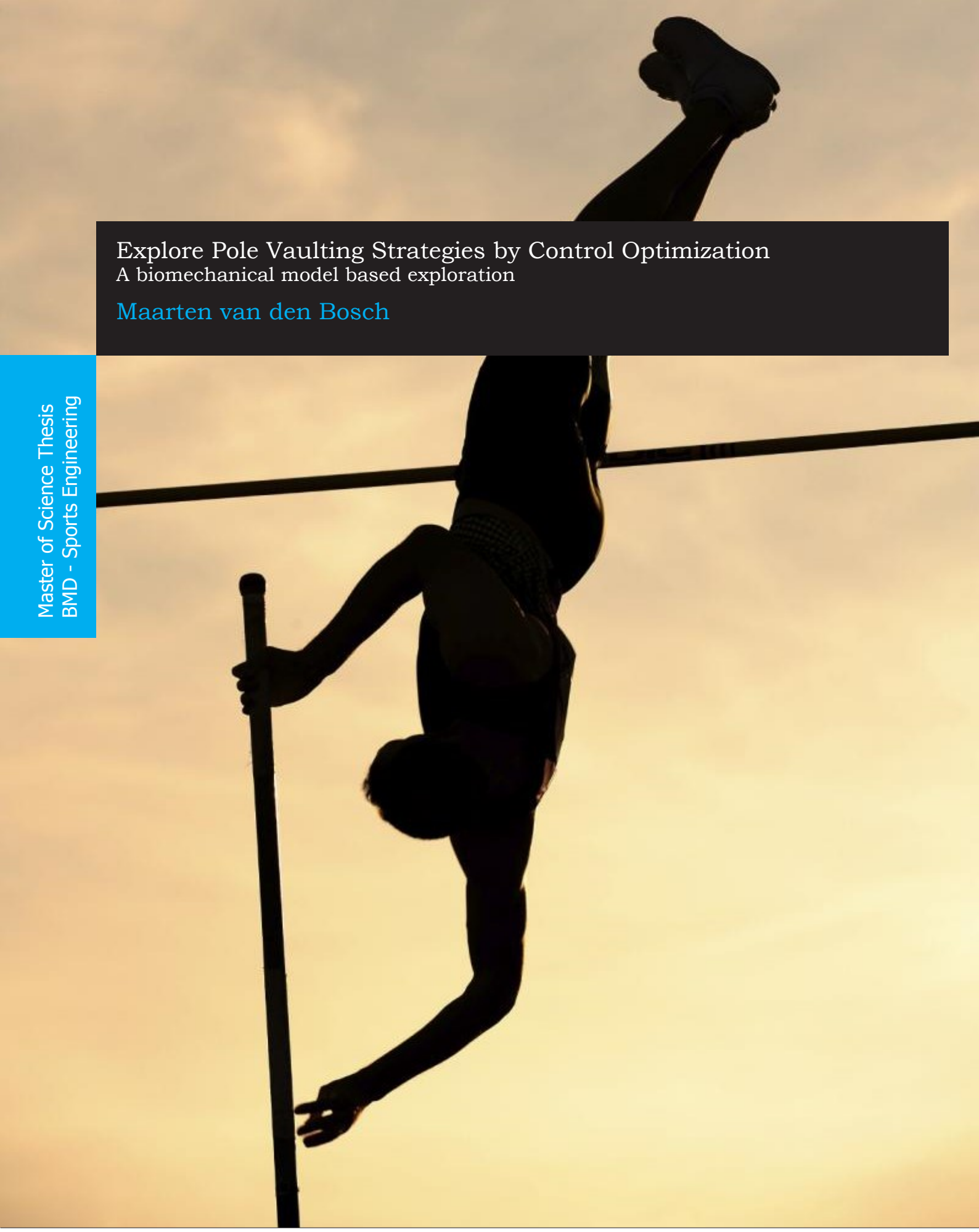

Explore Pole Vaulting Strategies by Control Optimization

A biomechanical model based exploration

Maarten van den Bosch

Master of Science Thesis
BMD - Sports Engineering

TU Delft Delft University of Technology

Challenge the future

Explore Pole Vaulting Strategies by Control Optimization

A biomechanical model based exploration

MASTER OF SCIENCE THESIS

For obtaining the degree of Master of Science in Mechanical Engineering
at Delft University of Technology

Maarten van den Bosch

October 11, 2018

DELFT UNIVERSITY OF TECHNOLOGY

Department of

BIOMECHANICAL ENGINEERING

The undersigned hereby certify that they have read and recommend to the Faculty of Mechanical, Maritime and Materials Engineering for acceptance a thesis entitled **"Explore Pole Vaulting Strategies by Control Optimization"** by **Maarten van den Bosch** in partial fulfillment of the requirements for the degree of **Master of Science**.

Dated: October 12, 2018

Chairman: _____
Prof.dr. F.C.T. van der Helm

Supervisor: _____
Dr.ir. O.K. Bergsma

Reader: _____
Dr. ir. Giuseppe Radaelli

Reader: _____
Dr.ir. A.L. Schwab

Contents

Reading Guide and Acknowledgements

Hear by I present my Master Thesis to fulfill the requirements for the degree of Master of Science. The core is written as a scientific article. More back ground knowledge of the build Matlab model are given in the Appendices afterwards.

In my first year in Delft, I doubted a lot if I had to quit with my Mechanical Engineering bachelors to become a physiotherapist. The human body fascinated me.And it still did after my bachelor. Picking a master was therefore an easy choice. I studied sports engineering for over three years, but it still fits like a glove.

The same goes for the topic of the thesis, the pole vault motion. It is almost an extreme sport with high velocities, big heights and many risks for the athlete. The combination with the mechanics of the pole still fascinates me.

I wish to thank my supervisors Frans van der Helm and Otto Bergsma. The anecdotes sports (how to make a pitcher more sensitive, how a darter throws his arrows) and/or other studies. The amount of knowledge and the discussions at our meetings where very inspiring. A special thanks is for Marco Reijne, for the weekly support. He often helped me out by pointing out the true important things and let less important stuff go for a while, to keep making progress.

I really gave this report all I had. I hope you will experience that while reading, enjoy!

Delft, The Netherlands 12-10-2018

Maarten van den Bosch

Explore Pole vaulting strategies by control optimization

Delft University of Technology
Maarten van den Bosch

October 12, 2018

Abstract

The development of the pole vaulting record is only improved by 1 centimeter over the last 25 years. Multiple studies show signs of different control strategies in elite pole vaulters, without pointing out what the cause of the differences is The aim of this research is to explore pole vaulting strategies by a control torque optimization. The optimization is performed for a simplified biomechanical model. The vaulter contains three segments: arms, a trunk including the head and legs. The joints are represented by torque actuators, located at the hands, shoulder joint and hip joint. The torque profile of each actuator is optimized. The optimization starts just after the pole is planted. It ends when the vaulter releases the pole. The pole length, pole stiffness, the vaulter's length, the vaulter's mass and the take-off angle are varied to discover the influence of these parameters on the control strategy. Three control strategies are found, as well as two power management strategies. Global trends are found. An increased pole stiffness, a decrease in length and mass of the athlete and a decreased take-off angle improved the performance. A possible optimal pole length is found.

Introduction

Pole vaulting is one of the most exciting track and field events. The vaulters entertain the audience by vaulting heights over 6 m, reached in less than two seconds. Where every vault is a thrilling event, the overall development of the discipline is much less exciting. Over the last 25 years, the world record has only increased by two centimeters without a clear cause why. In ten years before that, the world record increased over 30 centimeters as shown in figure 1.

To break the world record, the vaulter has to improve the height of the vault. In energy terms, the vaulter has to increase his potential energy at the end of the vault. The amount of potential energy is a result of the energy transformation of kinetic energy, gained during the approach, and strain energy, gained by bending the pole.

According to Brüggemann et al. [1999], the amount of kinetic energy and strain energy differs significantly among elite pole vaulters. Each vaulter seems to have his own strategy to perform his best vault. The cause of the difference in strategy is unknown.

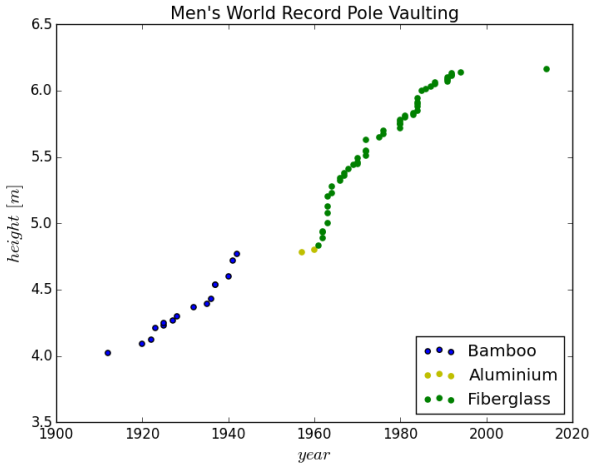

Figure 1: Time line of the development of the world record in men's pole vaulting. The colour of the dots indicates the matieral of the used pole. Remarkable is the sudden stop of the development of the world record. Source:IAAF website

The goal of this research is to improve the pole vaulting performance by exploring the motion strategy, or control strategy, of the athlete and the effect of the selection of the pole, using a simple biomechanical model. With more knowledge of the control strategy, the combination of vaulter, pole and control strategy can be optimized to increase the pole vaulting performance.

To improve the pole vault performance, the amount of potential energy at the end of the vault has to increase. To do so, the vaulter can either reduce the losses during the vault, execute the vault more efficient, or increase the amount of kinetic energy and strain energy during the vault. The approach to increase the total amount of

energy of the pole-vaulter system, differs per main phase of the vault. The pole vault motion contains four main phases: the approach or run-up, the take-off phase, the pole support phase and the fly-away phase.

The run-up phase is the start of the vault and ends at the vaulters second last ground contact. During the run-up phase, the vaulter can increase the amount of kinetic energy by increasing his final velocity.

Adamczewski and Perlt [1997] and Brüggemann et al. [1999] have shown a strong correlation between the final run-up velocity and the vaulted height. However, the studies of Adamczewski and Perlt [1997], Zagorac et al. [2008] and Linthorne and Weetman [2012] show no increase of the velocities of the vaulter's last stride over a period of two decades. The importance of the initial velocity is known by the athletes and coaches, and therefore well trained. Since the elite vaulters are most likely already at the limit for maximum run-up velocity, an increase of the run-up velocity to improve the world record seems not an option.

The second phase is the take-off phase. It starts at the second last ground contact of the vaulter and ends when the pole is planted and the vaulter loses ground contact. In this phase, energy is lost due to the non-elastic collision when the pole is planted. The loss of energy is estimated to be around 10% of the vaulter's energy at the start of the take-off phase. Neither tje pole nor the vaulter's body is able to store energy of the collision. The energy is damped out by the body of the vaulter.

According to Liu et al. [2011], the energy loss of the collision can be reduced by increasing the take-off angle. The take-off angle is the angle between the jump direction of the vaulter and the horizontal axis. The horizontal velocity decreases in that case, resulting in a smaller collision and thus less energy loss. Less elastic energy is stored in the pole, but by jumping up, the vaulter increases its potential energy. However, changing the direction of the velocity of the center of mass when jumping up, also results in a loss of velocity and thus in a loss of kinetic energy (Linthorne [2000],Linthorne et al. [2005]).

Another way to reduce the losses caused by the collision is to give the pole a slight pre-bend. The pre-bend reduces peak force at the collision, therefore, less energy is dissipated by the body of the vaulter. A big pre-bend reduces the upwards acceleration when the pole straightens.

The third phase is the pole support phase. It starts when the pole is planted and the vaulter loses ground contact. The vaulter can increase the energy in the system by actively bending the pole during the pole support phase. According to Frère et al. [2012a] an experienced vaulter with a personal best of 82% of the current world record of 6.16 meter, can gain an additional 22% of his initial energy. The initial energy is calculated as the sum of the potential and kinetic energy at the end of the approach, just before the pole is planted. The average initial energy of this study was 40 joules per kilogram body weight.

Brüggemann et al. [1999] performed an energy analysis of the vaults of the pole vault finals at the World Championships of 1997. He split the pole support phase into the pole bending phase and the pole straightening phase to get more insight in the control strategy of the athlete to gain energy. He found significant differences in control strategies, even though the subjects were all elite vaulters with similar run-up velocities. The differences in control strategy is a sign that the optimal control strategy is not found yet.

The elite vaulters in the study of Brüggemann reached an energy gain around 4.5% of their initial energy. The average initial energy in the study of Brüggemann was 57.03 Joules per kilogram body weight. The energy gain they developed is not close to the 22% Frère found. In absolute values, the vaulters in the study of Frère also perform better with an average of 8.8 Joules per kilogram body weight. The elite vaulters in the study of Brüggemann gained an average of 2.57 Joules per kilogram body weight. They are faster during the run-up phase but are less efficient during the pole support phase. Why this is the case is not known. If the elite vaulters could reach the efficiency to gain an additional 8.8 Joules per kilogram body weight, the world record would increase to 6.7 meters.

The last phase is the fly-away phase. It starts when the pole does not contribute to the vault anymore. The last thing the vaulter has to do is fly over the bar without touching it. There is not much room for improvement besides placing the bar as close as possible to the highest point of the vault.

Based on the current findings, the most promising phase to improve the pole vault motion by exploring different control strategies is the pole support phase. So, the period the biomechanical model simulates, starts after take-off and ends when the fly-away phase starts.

A significant improvement of the run-up is not possible since it is probably already maximized by elite pole vaulters. An improved take-off phase without controlling the period after take-off is also not effective. The position and velocity of the vaulter at the end of the take-off phase has probably an influence on the control of the vaulter and thus the final height.

Problem statement

The cause of the different motion strategies found by Brüggemann et al. [1999] is unknown. The variations are a

sign of a sub optimal combination of the pole, the vaulter and the strategy. To find the optimal combination of the pole, vaulter and strategy, a better understanding in the different motion strategies is needed. In this research, new insights will be obtained by optimizing the control strategy for different vaulter-pole combinations.

Aim of the research

A common approach to analyze the pole vault motion is by using inverse dynamical models. With that approach, the motion of multiple vaults is recorded to calculate the forces and torques used to execute the pole vault motion. The results can distinguish good vaults from bad vaults, but whether a certain vault was optimal for a pole-vaulter combination cannot be said with only inverse dynamical models.

With a forward dynamical model, the motion is a result of prescribed control forces. Multiple situations with different vaulter, pole and control strategy combinations can be simulated with forward dynamical models to find the vaulting performance.

An example of a forward dynamical model is build by Reijne [2016]. A mechanical pole vault model was build to test the potential of two vaulting pole innovations. The vaulter was simplified to two segments. The final movement was found with a trial-and-error approach. The true influence of a selected pole and control strategy on the vaulted height cannot be found with the model developed by Reijne [2016]. Due to the trial and error approach to form control strategies, it is not possible to compare different vaults, and hence different strategies, as it is unknown if for each vault the optimal control strategy, and hence maximum height, is achieved. To ensure maximum height is reached, the control strategy of each type of vault should be optimized.

The goal of this research is to provide the optimization of the control strategy of a simplified biomechanical model. The optimization is done with MATLAB 2017a using the optimizer `fmincon`. The aim is to maximize the final height with the optimal control strategy for a given pole-vaulter combination. The optimization space will be constrained as less as possible to include new possible control strategy.

A sensitivity analysis is performed to find the influence of pole properties and vaulter properties on the the control strategy. This is done by varying the initial properties of the vaulter and the pole and then find the maximal possible height by optimizing the control strategy. The initial properties of the vaulter are his length and mass. These parameters are varied to determine whether the control strategy is athlete specific or athlete independent. The initial properties of the pole are its length and its stiffness. These properties are varied to determine whether the different control strategies found by Brüggemann et al. [1999] is caused by selecting different poles.

A second sensitivity analysis is performed to find the influence of variations in the take-off angle on the control strategy. The take-off angle is varied to investigate the influence of the by Liu et al. [2011] suggested beneficial increase of take-off angle. The magnitude of the initial velocity is not adjusted. As stated in the introduction, the initial velocity is not changed over the last decades.

Methodology

A simple biomechanical model of the vaulter pole is made. The simulations start just after the pole is planted and the vaulter took off. The simulation ends when the pole is almost stretched.

Pole-Vaulter Representation

The pole vault motion during the pole support phase contains four main movements. The first movement is the swing-up, where the legs swing forward until the body is straight. Then, the rock-back starts. The vaulter tugs in his legs and rotates around his shoulder axes. The rock-back stops at the moment of maximal pole bend (MPB). During the stretch movement the vaulter stretches his legs and torso upwards, keeping his body as close to the pole as possible. The last movement is the pull up and starts when the legs are fully stretched. The vaulter pulls himself up and turns around his longitudinal axis. The pole support phase ends when the vaulter releases the pole and flies over the bar.

The main movements are clearly two dimensional. This is confirmed by Morlier and Cid [1996] who did a 3-dimensional angular momentum analysis of the pole vault motion. A third dimension is only necessary to describe the longitudinal rotation during the pole release phase and the rotation of the pole, to not jump into it. Schade et al. [2000] determined the difference of 2-dimensional and 3-dimensional calculated potential and kinetic energy of a vaulter. The calculations were based on video recordings. The difference between the 2-dimensional and 3-dimensional approach was less than 1 percent.

During the pole support phase, the arms are fully stretched until the pull-up. There are big rotations around the shoulder and the hip axis. The knees are bend during the rock-back movement and stretched in the movement

after that. Bending the knees results in a slight shift of the center of gravity but probably will not effect the amount of work the vaulter performs during the jump.

Based on the movement analysis and the findings of Morlier and Cid [1996] and Schade et al. [2000], a 2-dimensional representation is sufficient to get realistic insight in the pole vault motion. The number of segments of the vaulter is reduced to three: the arms, the head and torso, and the legs. The main rotations are covered but, the complexity, and therefore the computational time, is reduced. It also increases the simplicity of the model, which makes it better understandable.

In reality, the vaulter holds the pole with two hands which are 0.7 meters apart. The distance between the hands is relatively small to the length of the pole. The length of the pole can go up to 5 meters measured from tip to upper hand. The vaulter bends the pole by pushing with his lower hand and pulling with his upper hand. The elbow joint of both arms is extended until the pull up phase (Frère et al. [2012a]). Therefore, the arms are modeled as one segment without an elbow joint, attached with a hinge to the tip of the pole. The torque applied at the tip of the pole, the muscles at the shoulder joint and hip joint are represented by three torque actuators. So, the control forces described in the section Optimization, are represented by three control torque actuators.

The representation is shown in figure 2. The movement of the vaulter is described by five generalized coordinates: the position (x, y) of the center of mass of the arms, the angle of the arms (ϕ), the angle of the shoulders (θ) and the angle of the hips (ψ). The control torque actuators are the hand control torque, T_1, the shoulder control torque, T_2, and the hip control torque, T_3.

The model is very similar to the model build by Reijne [2016] who build for his master thesis a simple biomechanical pole vault model to test the potential of two vaulting pole innovations. The vaulter contained two segments. The final movement was found with a trial-and-error approach. The optimization of the improved model of Reijne makes it possible to find new movement strategies. More realistic vaults with different initial properties, such as pole length, can be compared.

Equations of Motion

The motion of the pole and the vaulter is calculated by a combination of an elastica model and the vaulter model.

The vaulter model contains the equations of motion to determine the accelerations of the vaulter as a result of the pole force, gravity and the torques at the hinges. The equations of motion are determined using the TMT-method, a combination of Newton-Euler method and the Lagrange

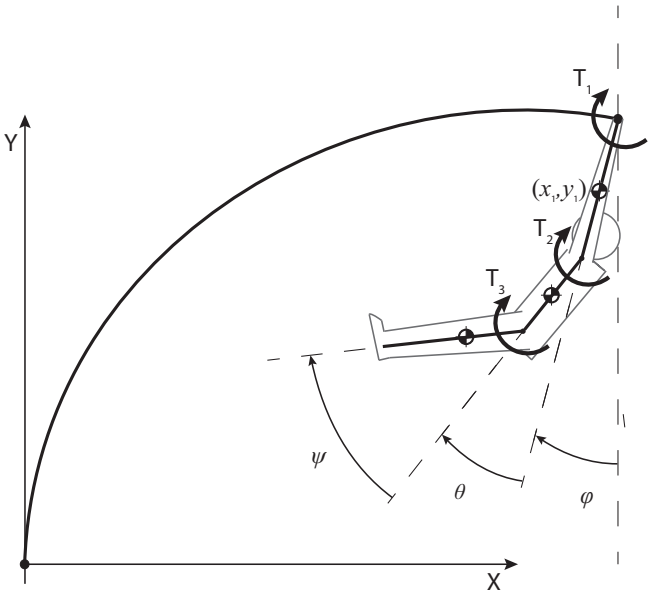

Figure 2: Simplified model representation. Generalized coordinates: the center of mass of the arms (x, y), the angle at the hands (ϕ), the angle at the shoulders (θ) and the angle at the hips (ψ). Control torques: T_1 is located at the top of the pole, T_2 is located at the shoulders, T_3 is located at the hips

method Schwab and Wisse [2001]. The derivation of the equation of motion is given in Appendix - Equations of motion.

The equations of motion are solved numerically using the fourth order Runge-Kutta integration scheme. The exact scheme and implementation in Matlab is given in Appendix - Numerical integration with the RK4-method.

The elastica model, or pole sub-model, is built by Reijne [2016]. The input variables are the pole length, pole stiffness, the torque at the tip of the pole and the distance from tip to tip. With elliptic integrals, the model calculates the reaction force on the vaulter and the shape of the pole.

Initial Conditions and Properties

The simulations start just after the pole is planted and the vaulter took off. So, the pole is already bent and the vaulter has no ground contact.

The exact initial position, given by the generalized coordinates of figure 2, the initial velocities, the pole length and take-off angle are based on the initial position of Ekevad and Lundberg [1995]. The pole stiffness is based on the used value of Reijne [2016].

The length, the mass, the location of the center of mass and inertia of each segment of the model is based on Moore et al. [2009]. The global inertia is variable during the vault, since the global center of mass of the vaulter shifts while moving (see Appendix - Inertia).

The amount of initial energy of the system is divided into elastic energy in the pole and kinetic and potential energy of the vaulter. The total amount of initial energy is constant for every set of initial conditions and initial properties. The amount is based on the average initial energy in Joules per kilogram body weight as Brüggemann et al. [1999] found. The initial energy was measured before the pole was planted. The simulation starts after the non-elastic collision of the pole plant. So, the expected energy loss of 10% is subtracted of the initial energy Brüggemann found. The resulting amount of energy is split up in pole energy, potential energy and kinetic energy according to the initial conditions of the generalized coordinates. The fraction linear kinetic energy determines the velocity of the vaulter.

For the sensitivity analyses, the pole length, pole stiffness, length of the vaulter, mass of the vaulter and the initial take-off angle are varied. A change in one of the properties disturbs the initial energy balance. An increase of the pole length, while keeping the initial position the same, results in a bigger amount of initial energy. In case of the pole length, the initial position is changed to compensate for the increased energy. The properties for the benchmark vault will have the values shown in table 1 and table 2. The properties of the vaulter are based on Moore et al. [2009]. The pole length and stiffness, the initial position and initial velocity are in accordance with Hubbard [1980]. The compensation of the other initial properties are described in more detail in Appendix - Matlab Model

Optimization

The model needs prescribed torque profiles for each control torque to perform a vault. The three control torques are time dependent and determine the strategy the vaulter uses. The control torques functions are represented as a sixth order polynomial. Each term is multiplied with a factor A to G. This form is chosen for its flexibility in shape compared to a spline function which Matlab is able to generate. The number of terms is based on a curve fit described in Appendix - Model. A sixth order polynomial is choosen to make complex profiles possible.

$$T_c(t) = At^6 + Bt^5 + Ct^4 + Dt^3 + Et^2 + Ft + G \qquad (1)$$

The implementation of the control torques into Matlab are found in Appendix - Model.

The seven optimization parameters A to G, which determines the control strategy, are given in equation 1. Each joint has its own control torque profile, so twenty-one parameters are optimized in total.

For the sensitivity analyses, the pole length is varied from 4.22 meters to 4.80 meters. The pole stiffness is varied from 2272 Nm^2 up to 2772 Nm^2. The length of the vaulter is varied from 1.68 meter to 1.92 meter. The mass of the vaulter is varied from 60 kilograms to 87 kilograms. The take-off angle is varied from 2.8 degrees to 19.8 degrees.

Objective

In energy terms, the vaulter wants to maximize the amount of potential energy at the end of his vault. The model excludes the pole release phase. So, the objective changes to the maximal sum of potential and upwards kinetic energy while holding the pole. The objective is maximized by optimizing the terms in the polynomial of the control torques of equation 1.

Final position

The resulting maximized energy of the vaulter is converted into a fictional final point in space. The body of the vaulter is transformed into a point mass, located at the center of mass of the vaulter when the maximal amount of energy is reached. The velocity of the point mass is found by the average kinetic energy in x- and y-direction of the three

Table 1: Initial properties of the vaulter model, l_1 to l_5 are the distances between joints and centers of mass of the segment, starting at the hands. See fig. B.1. The properties of the vaulter are based on Moore et al. [2009]. The pole length and stiffness are found in Hubbard [1980].

m_1	7.2	kg	I_1	0.22	kg m^2
m_2	41.6	kg	I_2	1.35	kg m^2
m_3	23.2	kg	I_3	1.59	kg m^2
l_1	0.27	m	l_2	0.34	m
l_3	0.20	m	l_4	0.28	m
l_5	0.40	m			
L	4.57	m	B	2522	Nm^2

Table 2: Initial conditions of the benchmark vault. The angle α is the take-off angle, the angle between the horizontal axes and the velocity vector as a result of $\dot{x}_{cm}$ and $\dot{y}_{cm}$. The initial position and initial velocity are in accordance with Hubbard [1980].

x_{cm}	3.57	m	$\dot{x}_{cm}$	8.7	m/s
y_{cm}	1.12	m	$\dot{y}_{cm}$	1.2	m/s
ϕ	0.4	rad	$\dot{\phi}$	0.4	rad/s
θ	0	rad	$\dot{\theta}$	0	rad/s
ψ	0	rad	$\dot{\psi}$	0	rad/s
α	7.85	deg			

body segments. The final position is extrapolated with known x- and y- position and velocity. The exclusion of the pole release phase, or fly-away phase, has no significant effect on the energy transformation. As stated by Frère et al. [2012b], the performance of a vaulter is not likely influenced by the final actions of the vault. However, the constraint to move an entire body over the bar is heavily simplified. Favourable positions to complete a successful vault are neglected.

Constraints

The constraints of the optimization are chosen such that the resulting vaults are feasible vaults. The constraints are divided into two groups. The first group are physical bounds of the pole vault motion. The group contains constraints on joint angles,the physical space the vaulter can move in, so that elements will not go through the ground or are out of reach of the pole. The second group are bounds to ensure a realistic vault. They describe the shape of the pole, the maximal torque per joint and the maximal power per joint.

The vaulter is not infinitely strong which make maximal and minimal magnitude bounds of the control torques necessary. Based on torque profiles found in Morlier and Mesnard [2007], the torque at the tip of the pole is bounded by +600 Nm and -600 Nm. After the pole is maximal bent, the bounds narrow linearly to +100 Nm and -100 Nm. The absolute control torque bounds of the shoulders and hips are 500 Nm and 300 Nm respectively. The maximal absolute control torques are found in McGinnis [1989] who obtained the magnitudes by measurements on elite pole vaulters.

The only muscle property introduced, is the maximal amount of power the shoulders and hips can deliver. The power bounds are determined by running multiple optimizations for different pole length and pole stiffness. The final performance where unrealistic with final heights of twice the world record. This was caused by a raise in power of 5000 Watts in the last 0.3 seconds of the vault for both the shoulders and the hips as shown in figure 3.

The period before the excessive peak at the end did not show extreme values of angular velocity or power. The power peaks in this period where below 2000 Watts at the shoulders and below 2500 Watts at the hips (see fig. 3). These absolute power constraints are implemented in the optimization procedure to ensure a more realistic combination of control torque and angular velocity.

There are no muscle properties incorporated besides the power bounds. The control torques are in reality dependent of both the angle of the joint and the angular velocity of the joint. There are no studies found where

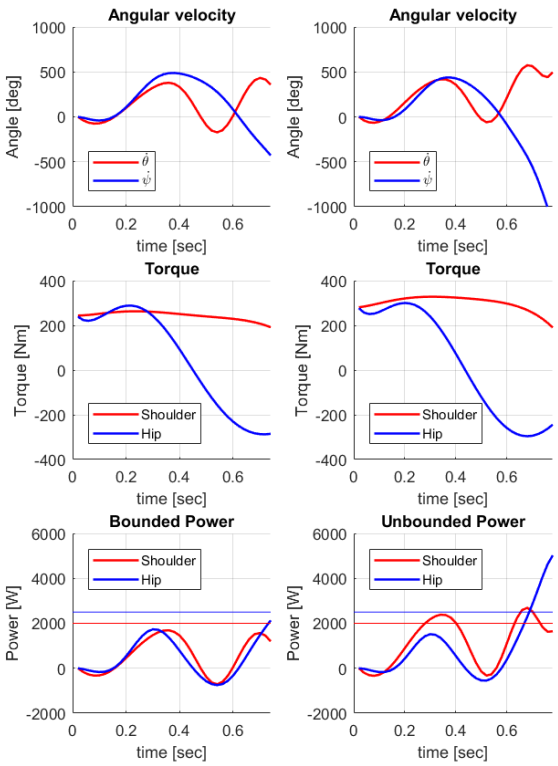

Figure 3: Example of a power bounded and a power unbounded optimization. The graphs on the left are bounded by a maximal shoulder power of 2000 Watts and a maximal hip power of 2500 Watts. The graphs on the right are unbounded. The increase of power over the last 0.2 seconds of the vault is very unrealistic. The power-bounded torque profile results in a vault of 6.22 meters. The power-unbounded torque profile results in a vault of 7.11 meters.

the maximal torque at the top of the pole, the shoulders or the hips is described in a torque-position-velocity relationship. An estimation of such a relationship can not be scientific supported and is therefore not made. The ability to generate a certain torque is not bounded by a prescribed torque-angle or torque-angular velocity relationship.

The last constraint is the x-position of the position where the maximum height is achieved, as described above. According to the IAAF competition rules 2018-2019, vaulters are allowed to place the bar between straight above the planting box and 80 centimeters behind the planting box. The maximal height the point mass reaches, has to be in this region to complete an optimal and valid vault.

A list of the constraints is described in Appendix - Model.

Initial Guess

The initial guess of each optimization is unique for each set of parameters. The initial guess is found by the same optimization script, without a formulated objective. The optimization is only focused on fulfilling the constraints. The constraints are made stricter to make sure the initial guess is not located at a constraint boundary. After running this script, an initial guess is formulated which fulfills all the constraints.

Results

The results of the sensitivity analyses are presented in depth for the variation of the pole stiffness. The analysis of the pole stiffness will form a guide for the analyses of the pole length, the vaulter's mass, the vaulter's length and the take-off angle.

The optimizer finds only around 40% of all the optimized situations a minimum. The other 60%, the optimizer converges to an infeasible point. Around 90% of the infeasible solutions, the biggest constraint violates is in the order of 0.5% of the constraint magnitude. A vault is called feasible when the biggest constraint violation is below 0.1 %.

The last feasible iteration of the infeasible optimized situation, is taken as the solution. The difference of the objective function of the infeasible solution and the last feasible iteration is typically around 3%.

Pole Stiffness

The stiffness of the pole is varied from 2272 Nm^2 up to 2772 Nm^2 with steps of 25 Nm^2. The following general trend found is: 'the stiffer the pole, the better the performance'. As shown in figure 4, the increase in vaulted height is mainly caused by an increase of the upward velocity at pole release. All the optimized vaults are divided into three strategies.

The final performances are remarkably high. The best vaulting performance is 7.42 meters, vaulted with a pole stiffness of 2722 Nm^2. The world record of 6.16 meters is broken with 1.62 meters.

Global Strategies

Varying the stiffness results globally in three different strategies, shown in figure 5.

Strategy one is called the 'Extension-strategy'. The strategy is found from $B = 2272 N m^2$ up to $B = 2372 N m^2$. The vaulted heights vary from 6.01 meters up to 6.33 meters. Characteristic for this strategy is the final position of the legs. These are always close to horizontal, either by an extended hip joint, an extended shoulder joint, or a combination of the two. The legs are extended to decrease the horizontal velocity which is typically higher at lower pole stiffnesses, as shown in figure 4. The horizontal legs results in a low center of mass compared to the other vaults, as shown in figure 4. The low stiffness of the pole results in a lower upward velocity at the end of the vault, partly due to its lower stretching velocity.

A second strategy is found at two stiffnesses over the entire interval. This strategy is called the 'Flexion-strategy', also shown in figure 5. The strategy is found at $B = 2572 N m^2$ with a final vaulted height of 6.86 meters and $B = 2697 N m^2$ with a final vaulted height of 7.08 meters. Characteristic for this strategy is the lack of shoulder and hip extension. The arms are almost aligned with the trunk and the hip has an angle around 90 degrees at the moment of pole release.

Strategy three is called the 'Upwards-strategy'. The strategy is found from $B = 2397 N m^2$ up to $B = 2772 N m^2$. The vaulted heights vary from 6.68 meters up to 7.42 meters. Characteristic for this strategy is the small shoulder flexion, combined with a big hip extension. As a result, the feet point upwards at pole release.

Control Torque profiles

The variation in control torque profiles over the range of pole stiffnesses is shown in figure 6. The 'Extension Strategy' shows the worst performance, varying from 6.01 up to 6.33 meters. The 'Flexion Strategy' cannot be clearly distinguished from the 'Upwards strategy based on the control torque profiles.

The control torque profile located at the hands of the vaulter show are very consistent up to $B = 2572 N m^2$, where the magnitude of the control torque for the first time switches from negative to positive. The same goes for the shoulder control torque profiles. Until $B = 2572 N m^2$, the shoulder control torques start flat. The control torque profile starts to decrease after 50 % of the vault is completed. At $B = 2572 N m^2$ and higher sitffnesses, the control torque profile switches back and forth from the a flat profile to a bow profile. The hip control torque profile is very consistent. The main variation is found in the last 20% of the vault. The cause of these differences is not found.

The control torque profiles are found in figure 6. The power profiles are given in figure 7. Remarkable is the increase of the number of oscillations in the power plot. It shows the importance of the timing of stretching the body to increase the upward velocity.

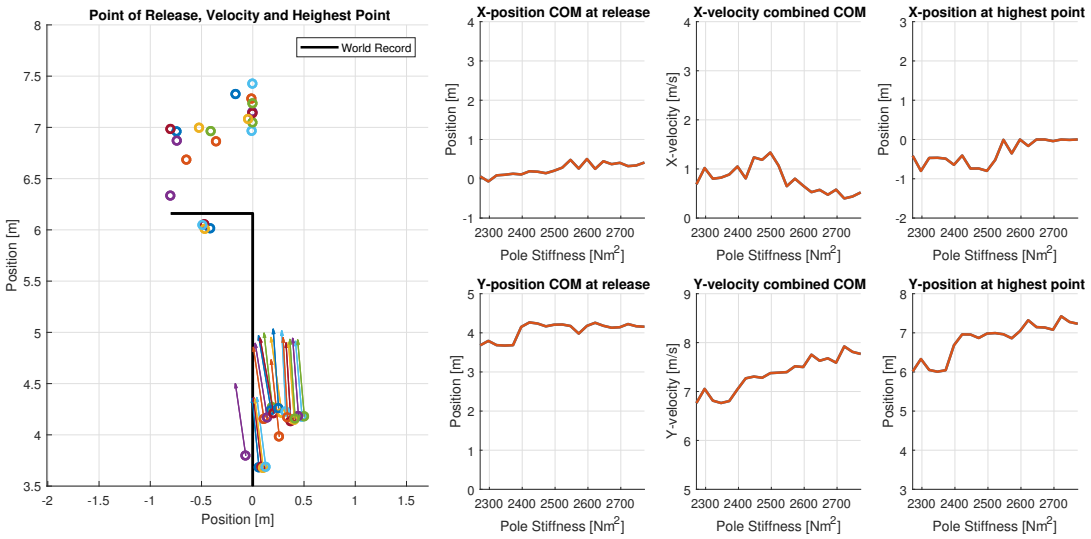

Figure 4: The final conditions at the end of each vault at pole release and final performance per pole stiffness in $N\,m^2$. On the left: the position and flying direction of the center of mass (COM). The small graphs on the left: the x- and y-position of the COM at pole release. In the middle: horizontal and vertical velocity of the COM at pole release. On the right: the horizontal position of the COM the highest point. Note: the bar placement is bounded by the region between -0.8 meter and 0 meter.

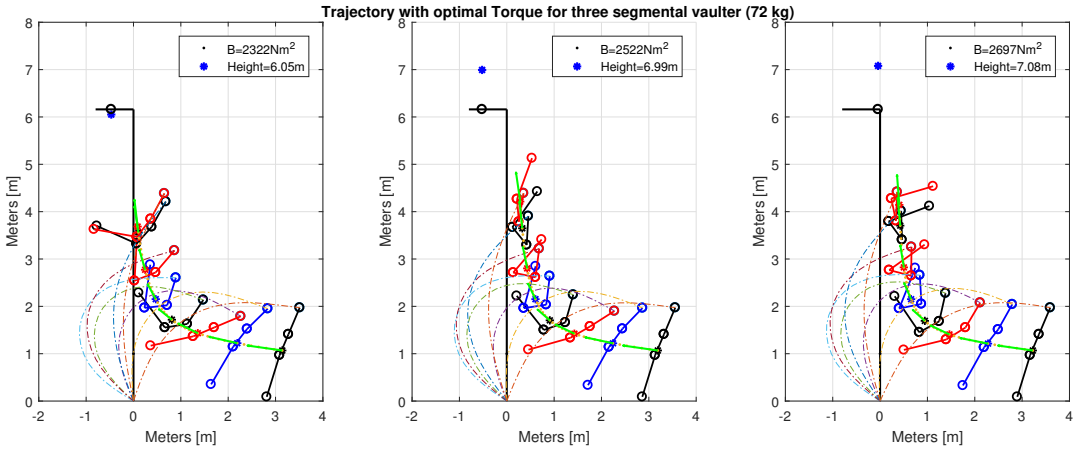

Figure 5: The three strategies found by varying the pole stiffness.
On the left: the 'Extension-strategy', found from $B = 2272N\,m^2$ up to $B = 2372N\,m^2$. The vaulted heights vary from 6.01 meters up to 6.33 meters. Characteristic is the final position of the legs which is close to horizontal.
In the middle: the 'Upwards-strategy'. The strategy is found from $B = 2397N\,m^2$ up to $B = 2772N\,m^2$. The vaulted heights vary from 6.68 meters up to 7.42 meters. Characteristic is the small shoulder flexion, combined with a big hip extension. As a result, the feet point upwards at pole release.
On the right: the 'Flexion-strategy'. The strategy is found at $B = 2572N\,m^2$ with a final vaulted height of 6.86 meters and $B = 2697N\,m^2$ with a final vaulted height of 7.08 meters. Characteristic is the lack of shoulder and hip extension. The arms are almost aligned with the trunk and the hip has an angle around 90 degrees at the moment of pole release.

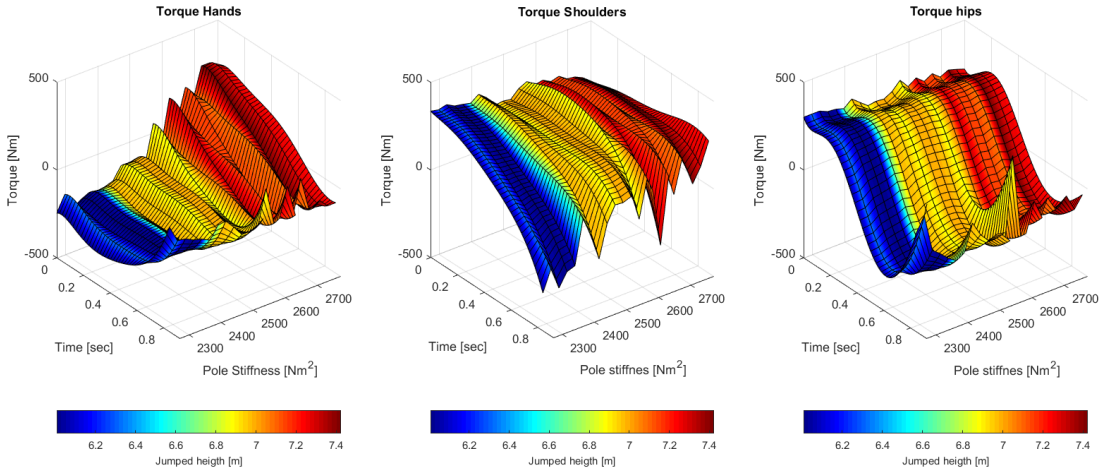

Figure 6: Optimized control torque profiles for pole stiffnesses varied from 2272 N m^2 to 2772 N m^2. On the left, the torque applied at the tip of the pole. In the middle: the torque applied at the shoulders. On the right: the torque applied at the hips. Note: the color represents the jumped height. The minimum height is 6 meters, the maximum height is 7.4 meters. A very global trend is found, the stiffer the pole, the better the performance.

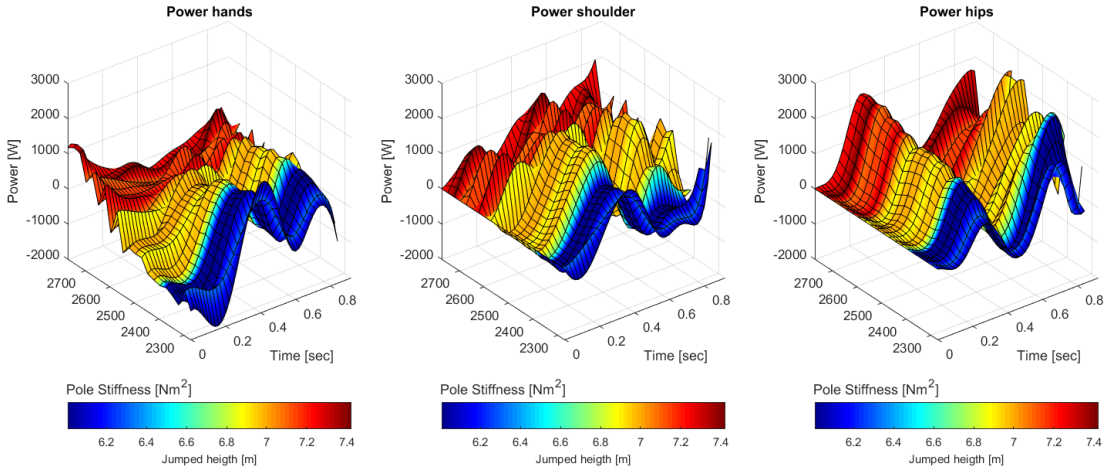

Figure 7: Power in Watts, developed per control torque. On the left: power generated at the tip of the pole. In the middle: power generated by at the shoulders. On the right: power generated at the hips. Note: the color represents the jumped height. The minimum height is 6 meters, the maximum height is 7.4 meters. The axis are changed compared figure 6 to increase readability.

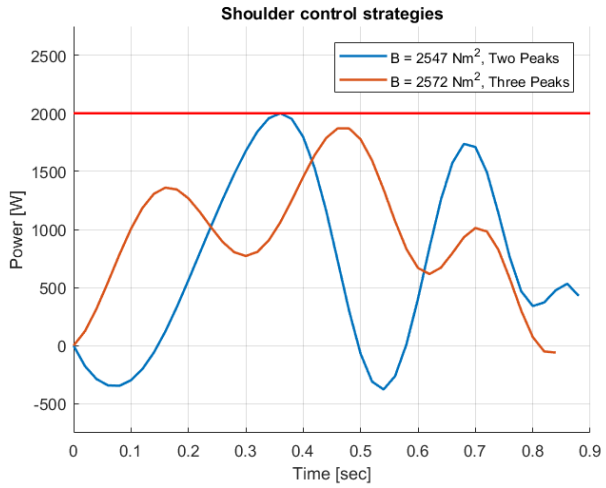

Figure 8: Power profiles as a result of the shoulder control strategy are shown above. 'Two Peaks' is found at a pole stiffness of $B = 2547 N\,m^2$, resulting in a vaulted height of 6.96 meters. 'Three Peaks' is found at a pole stiffness of $B = 2572 N\,m^2$, resulting in a vaulted height of 6.86 meters. The red line indicates the power constraint of 2000 Watts.

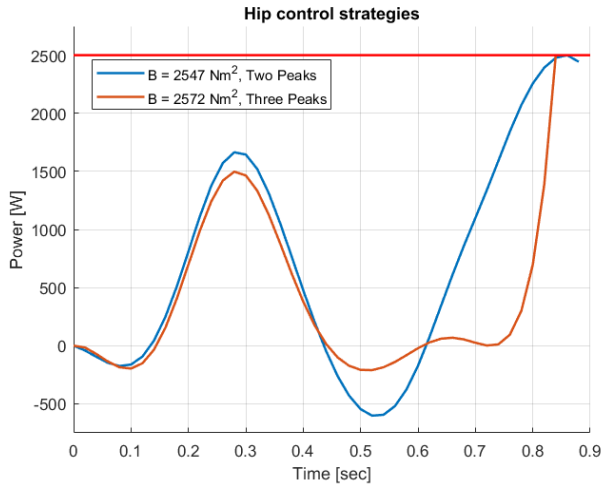

Figure 9: Power profiles as a result of the hip control strategy are shown above. 'Two Peaks' is found at a pole stiffness of $B = 2547 N\,m^2$, resulting in a vaulted height of 6.96 meters. 'Three Peaks' is found at a pole stiffness of $B = 2572 N\,m^2$, resulting in a vaulted height of 6.86 meters. The red line indicates the power constraint of 2500 Watts.

Power Management

The Upwards-strategy is found over a big range of stiffnesses. Based on very global criteria which are used above to describe the strategies, the Upwards-strategy is one strategy. The control torque profiles showed a consistency until B=2572 $N\,m^2$. A power analysis gives more insight in cause of different strategies. The power production of each control torque is shown in figure 7. The power is found when the control torque is multiplied by the angular velocity of the corresponding angle. It shows at which moment in time a control torque produces energy. Based on the produced power per control torque, the strategy is splits up into two control strategies.

The power profile from $B = 2272 N\,m^2$ up to $B = 2547 N\,m^2$ shows consistency for each control torque,each profile contains two positive peaks. The magnitude of the power peaks at the hands slowly decreases where the power at the shoulders and hips slowly increases.

At $B = 2547 N\,m^2$, the power profile of the shoulder control torque, suddenly changes. At this point, the control strategy switches back and forth between two different forms. The strategies are shown in figure 8. Remarkable is the small difference in pole stiffness.

The first control strategy, 'Three Peaks', contains three power peaks which stay all three below the maximal value of 2000 Watts. The second control strategy, 'Two Peaks', contains two power peaks where the first peak hits the maximal 2000 Watts.

The change in strategy is caused by hitting the shoulder power constraint. To improve the height, the vaulter changes his power management by spreading out the power production over three peaks with a lower magnitude compared to 'Two Peaks'. The result is a higher average power production. The average power production of 'Three Peaks' of figure 8 is 941.5 Watts. The average power production of 'Two Peaks' is 697.02 Watts. 'Two Peaks' compensates the lower amount of shoulder power by more hip power. As shown in figure 9, the power production higher for 'Two Peaks' with an average power production of 709.3 Watts against 365.5 Watts produced with 'Three Peaks'.

Improving the vaulting performance using the strategy 'Two Peaks' for stiffer poles is blocked by the constraint on the maximal shoulder power production. As a result, the strategy slowly merges into the 'Three Peaks' strategy. The merging process is illustrated for the shoulder power production in figure 10 and for the hip power production in figure 11. The power profile of the hands did not show a clear merging process.

The stiffnesses which are not shown in figure 10 and figure 11 did not take part in the merging process and showed a true 'Three Peaks' power strategy. This is further treated in the section Discussion.

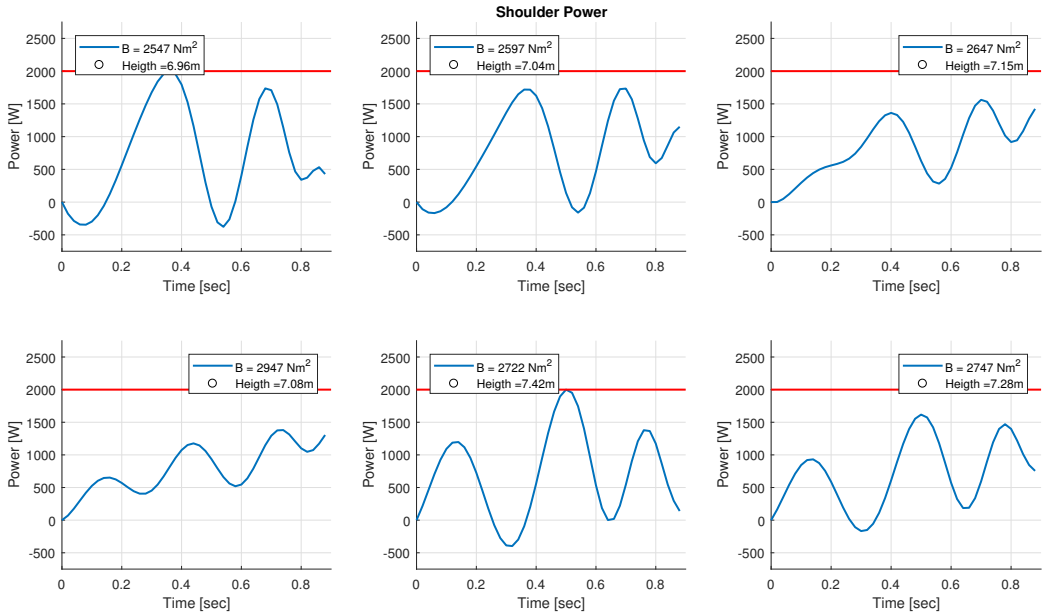

Figure 10: On the top left, the last true 'Two Peaks' strategy is shown. While moving from the left to the right and top to bottom, the third peak is growing while the maximal power peak decreases. The figure in the middle on the bottom row shows the best vault and is a full 'Three Peaks' strategy. The power profile shown on the bottom right preforms less. This could be caused by the bad convergence as described above.

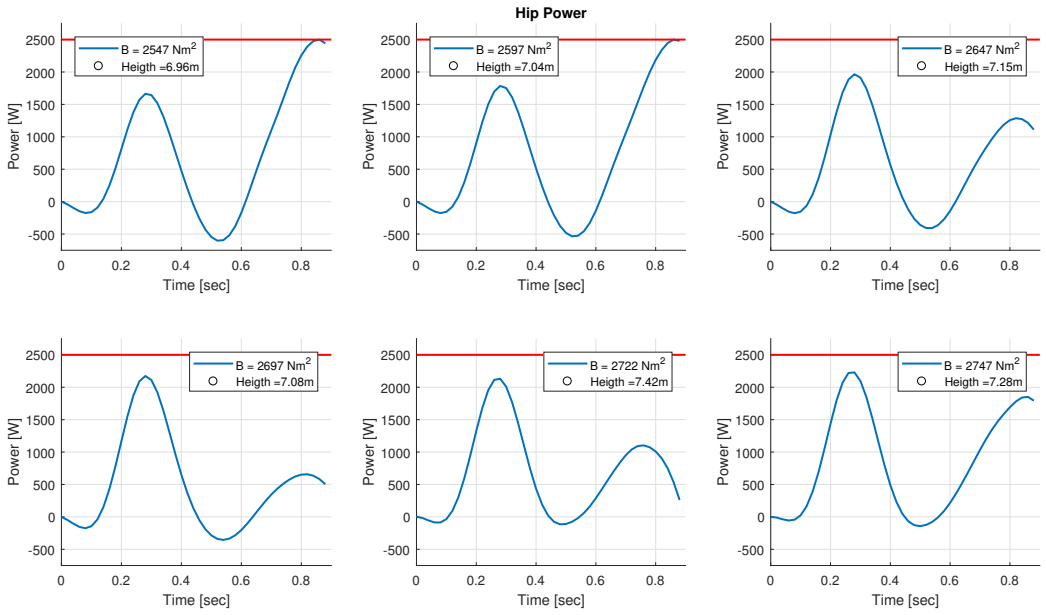

Figure 11: On the top left, the hip power profile matching the 'Two Peaks' strategy is shown. While moving from the left to the right and top to bottom, the first hip power peak increases, while the second peak first decreases and later on again increases. The figure in the middle on the bottom row shows the best vault and is a full 'Three Peaks' strategy. The power profile shown on the bottom right preforms less. This could be caused by the bad convergence as described above.

Energy

An energy analysis is performed to clarify what component is dominant in the objective energy. The objective is formulated as the sum of potential energy of the global center of mass and upwards kinetic energy of the global center of mass. As stated in the introduction, the energy kinetic energy gained during the run-up, is transformed into strain energy in the pole, which is returned to the vaulter as potential- and upward kinetic energy. So, the main components in the energy analysis are kinetic energy in x- and y-direction of the center of mass, the potential energy of the center of mass and the amount of energy stored in the pole.

The amount of energy stored in the pole is calculated as the sum of the initial energy and the total amount of work of each control torque minus the potential energy, kinetic energy and angular kinetic energy of the vaulter. The energy profile of each main component is shown in figure 12.

Figure 4 shows the same results as figure 12. Besides the 'Extension' strategy, all vaults have the same amount of potential energy at the end of the vault. The difference in height is a result of a higher amount of upward kinetic energy. The maximum amount of energy stored in the pole increases for stiffer poles.

The effect of the different power profiles is only found in the amount of performed work. Again, the back and forth switching from a 'Two Peaks' to a 'Three Peaks' strategy is visible. The other three energy components, the potential energy, the upward kinetic energy and the energy stored in the pole are very consistent.

Remarkable is the final negative amount of energy stored in the pole at the end of the vault. The amount of negative energy is the pole is further discussed in the section Discussion.
In the introduction, an energy gain of 22% of the initial energy is found among experienced vaulters by Frère et al. [2012a]. Brüggemann et al. [1999] found an energy gain of 4.5%. In figure 13 is the energy gain of the model presented. The model realizes a much bigger energy gain with peaks around 40%.

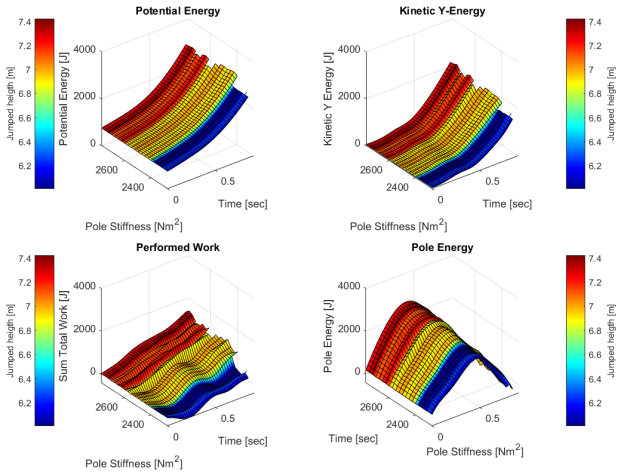

Figure 12: The amount of energy of each main energy component: potential energy, upward kinetic energy, the amount of performed work and the amount of energy stored in the pole. Besides the 'Extension' strategy, all vaults have the same amount of potential energy at the end of the vault. The difference in height is a result of a higher amount of upward kinetic energy. The maximum amount of energy stored in the pole increases for stiffer poles. The vaulted height is indicated by the color. The performance varies from 6 meters up to 7.4 meters.

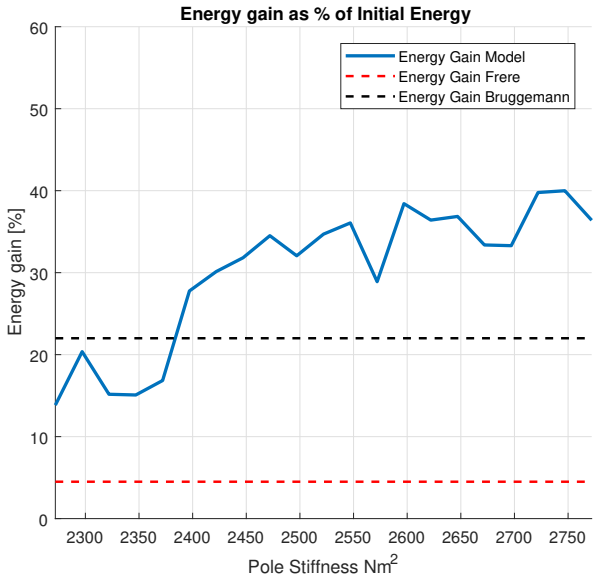

Figure 13: The energy gain of each vault as a percentage of the initial energy. The model realizes a much higher energy gain than the average energy gain found by Frère et al. [2012a] and Brüggemann et al. [1999]

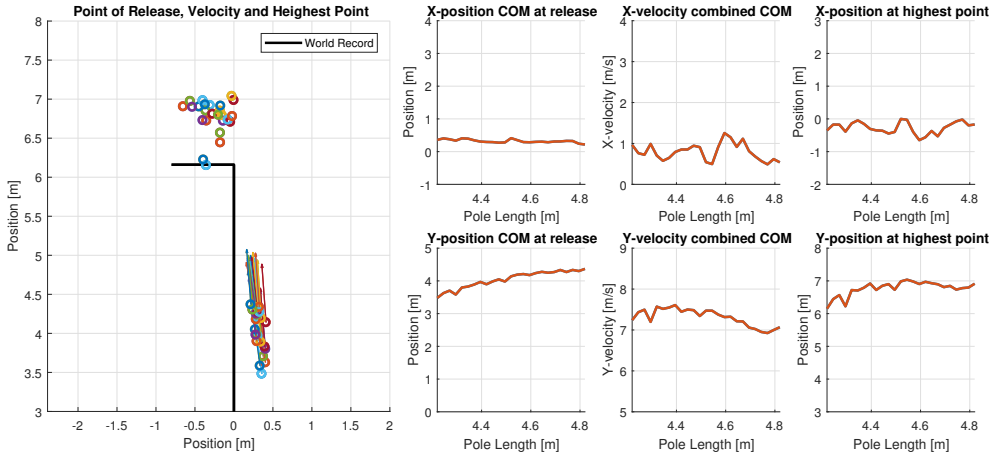

Figure 14: The final conditions at the end of each vault at pole release and final performance, per pole length in meters. On the left: the position and flying direction of the center of mass (COM) The small graphs on the left: the x- and y-position of the COM at pole release. In the middle: horizontal and vertical velocity of the COM at pole release. On the right: the horizontal position of the COM the highest point. Note: the bar placement is bounded by the region between -0.8 meter and 0 meter.

Pole Length

The pole length is varied from 4.22 meters up to 4.82 meters with steps of 2.5 centimeters. The model is very stable in its behaviour when the pole length is changed. There are no different control strategies found. Only the 'Upwards' strategy is found. The positions at pole release, the velocity at pole release and the final highest point are shown in figure 14.

Short poles result in a higher upward velocity. Long poles have as an advantage the increase of potential energy at pole release. The optimal pole length is found at 4.545 meters with a height of 7.03 meters.

The optimized control torques are shown in figure 15. The power production and main energy components are similar to the presented power production and main energy components of the first consistent part of the pole stiffness analysis.

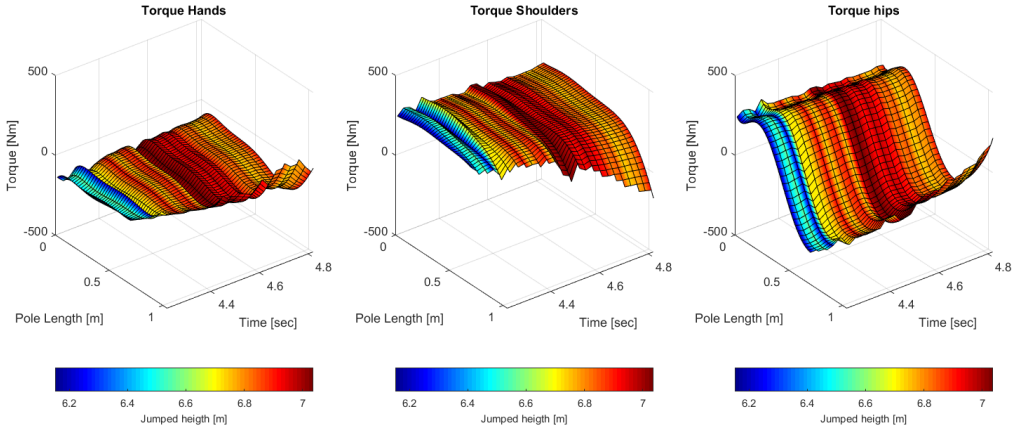

Figure 15: Optimized control torque profiles for pole length varied from 4.22 meters to 4.82 meters. On the left, the torque applied at the tip of the pole. In the middle: the torque applied at the shoulders. On the right: the torque applied at the hips. Note: the color represents the jumped height. The minimum height is 6.2 meters, the maximum height is 7.03 meters. According to these outcome, the optimal pole length is 4.545 meters.

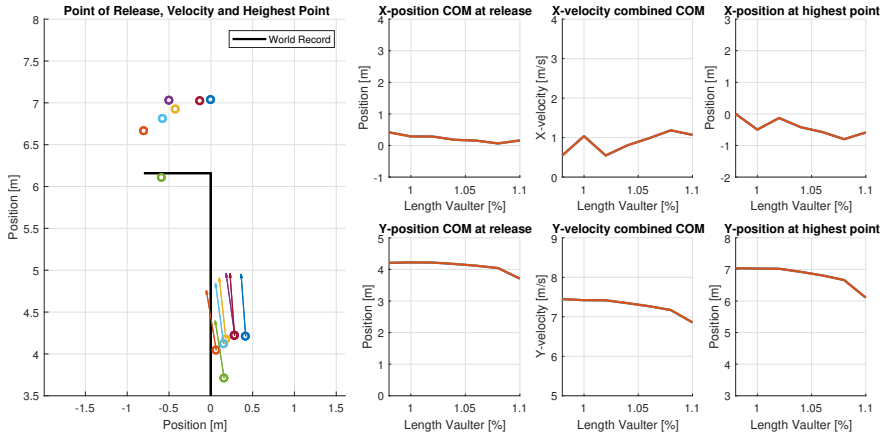

Figure 16: The final conditions at the end of each vault at pole release and final performance, per length of the vaulter in % of the benchmark length (Table 1. On the left: the position and flying direction of the center of mass (COM) The small graphs on the left: the x- and y-position of the COM at pole release. In the middle: horizontal and vertical velocity of the COM at pole release. On the right: the horizontal position of the COM the highest point. Note: the bar placement is bounded by the region between -0.8 meter and 0 meter.

Length of the Vaulter

The length of the vaulter is varied in % of the benchmark length, given in table 1. The segment length, given in Moore et al. [2009], are after neglecting the feet, hands and neck. The true length is therefore estimated at 1.75 meters. The length is varied from a decrease with 2%, which corresponds to a length of 1.72 meters, up to an increase of 10%, which corresponds to a length of 1.95 meters.

The following global trend is found: 'The shorter the vaulter, the better the performance'. A shorter vaulter has a lower inertia which gives him the ability to change his posture with less effort. The highest vault of 7.04 m is performed by the vaulter of 1.72 meters. The positions and velocity at pole release and the final highest point are shown in figure 16.

There are no different control strategies found. The 'Extension' strategy is found ones, at the maximal length of 1.95. The shoulder control torque and hip control torque necessary to point the feet up are beyond the constrained values. The vaulter is thereby forced to perform the 'Extension' strategy. The other vaults are executed with the 'Upwards' strategy.

The optimized control torques are shown in figure 17. The power production and main energy components are similar to the presented power production and main energy components of the first consistent part of the pole stiffness analysis.

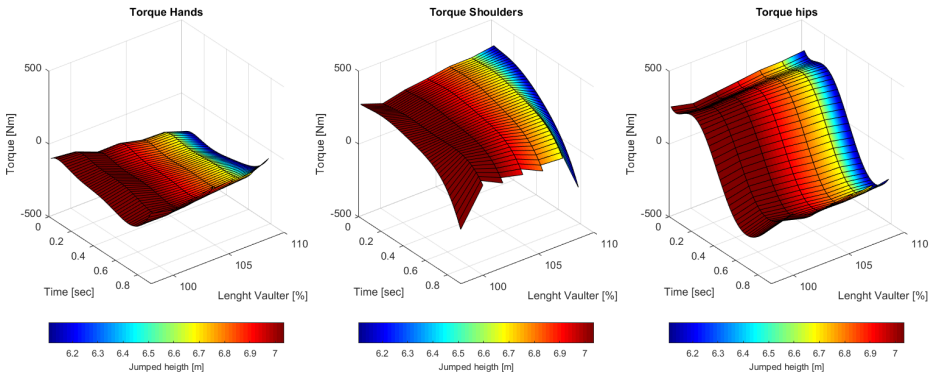

Figure 17: Optimized control torque profiles for the varied length of the vaulter over a range of 98% up to 110% of the benchmark length (Table 1. On the left, the torque applied at the tip of the pole. In the middle: the torque applied at the shoulders. On the right: the torque applied at the hips. Note: the color represents the jumped height. The minimum height is 6.1 meters, the maximum height is 7.03 meters.

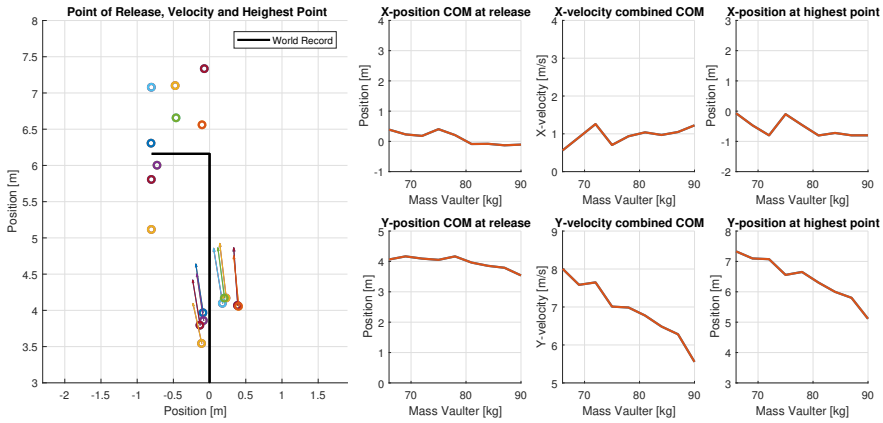

Figure 18: The final conditions at the end of each vault at pole release and final performance, per mass of the vaulter. The mass is varied from 66 kilograms up to 90 kilograms. The benchmark weight is 72 kg. On the left: the position and flying direction of the center of mass (COM) The small graphs on the left: the x- and y-position of the COM at pole release. In the middle: horizontal and vertical velocity of the COM at pole release. On the right: the horizontal position of the COM the highest point. Note: the bar placement is bounded by the region between -0.8 meter and 0 meter.

Mass of the Vaulter

The mass of the vaulter is varied from 66 kilograms up to 90 kilograms. The model is very sensitive for changes in the vaulter's mass, as shown by the inconsistent torque profiles of figure 19. A global trend however, is found: 'The lighter the vaulter, the better the performance.'

As shown in figure 18, vaulters with a lower mass score beneficial for both the height of the center of mass at pole release, as well as the upward velocity. The best vault is performed by the lightest vaulter of 66 kilograms with a final height of 7.33 meters.

All the different control strategies are found. The 'Extension' strategy is found after a weight of 78 kilograms. Again. The amount of torque necessary to point the feet up to complete the 'Upwards' strategy, is bounded, which leaves the vaulter with the 'Extension' strategy. This is in accordance to the increase in body length. When the mass increases, the inertia also increases. More effort is needed to get into the 'Upwards' position.

The different power management strategies are also found. After the mass below 72 kilograms, the torque profiles start to change drastically. Again, the power profile gives a clearer representation of the energy transmissions.

A change in mass does not lead to remarkable change of the energy components as discussed for the pole stiffness.

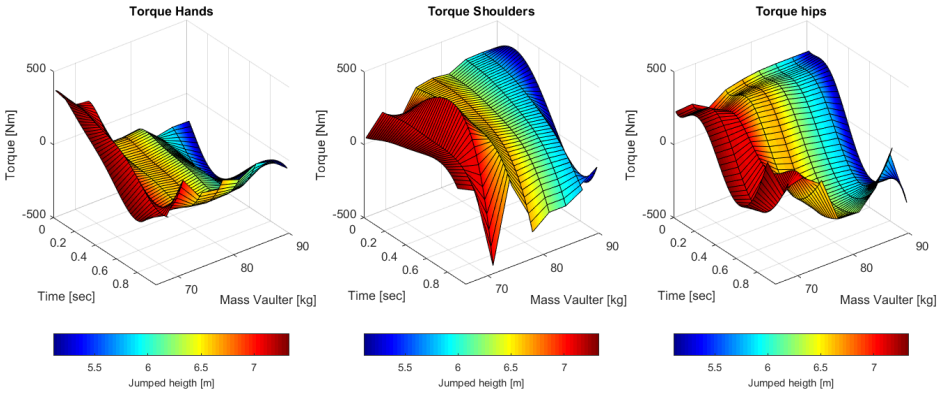

Figure 19: Optimized control torque profiles for the varied mass of the vaulter over a range of 66 kilograms up to 90 kilograms. The benchmark weight is 72 kilograms. On the left, the torque applied at the tip of the pole. In the middle: the torque applied at the shoulders. On the right: the torque applied at the hips. Note: the color represents the jumped height. The minimum height is 7.33 meters, the maximum height is 5.11 meters.

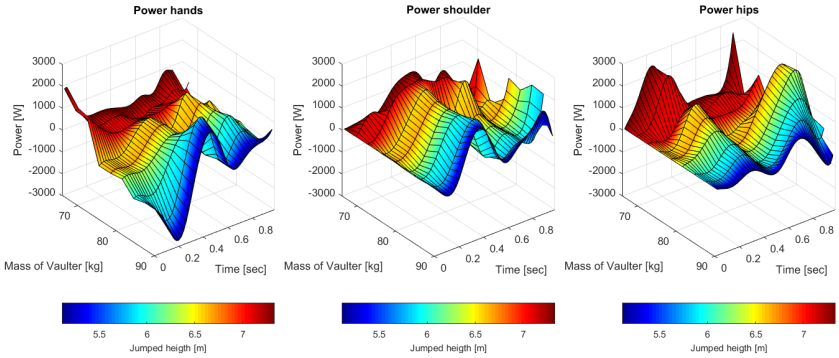

Figure 20: Power profile after optimizing the control torques for a range of body mass from 66 kilograms up to 90 kilograms. The change in power management is clearly visible as the power profiles at a body mass of 66 and 69 kilograms show three peaks, where the profiles after that show the 'Two Peaks' strategy.

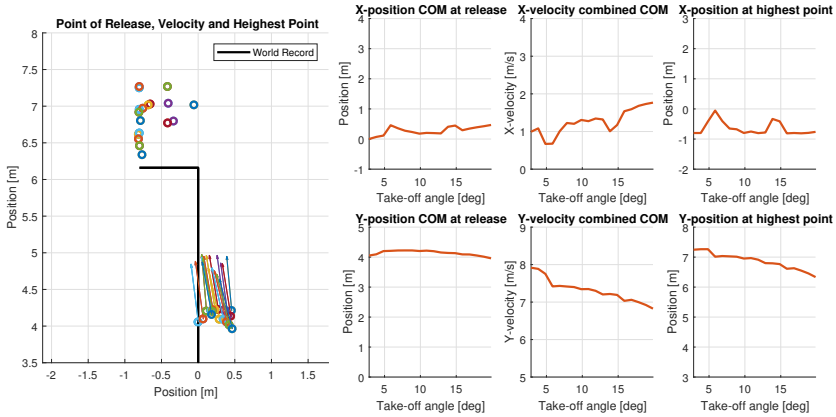

Figure 21: The final conditions at the end of each vault at pole release and final performance, take-off angle. In the middle: horizontal and vertical velocity of the COM at pole release. On the right: the horizontal position of the COM the highest point. Note: the bar placement is bounded by the region between -0.8 meter and 0 meter. The take-off angle is varies over a range of 3 degrees up to 20 degrees with steps of 1 degree. The best performance is found with the smallest take-off angle, 5 degrees. The vaulted heigth is 7.26 meters. An increase of the take-off angle results in a higher horizontal velocity. Less horizontal kinetic energy is converted into potential energy and upwards kinetic energy.

Take-off Angle

The best performance is found with the take-off angle of 5 degrees. The vaulted heigth is 7.26 meters. An increase of the take-off angle results in a higher horizontal velocity, as shown in figure 21.

Varying the take-off angle showed only the 'Upwards' strategy. For a take-off angle below 6 degrees showed the switch to the 'Three Peaks' power strategy. The optimized control torque profiles are shown in figure 22

An increase in take-off angle results in less energy transformation. This is shown by figure 23. More energy is directly transferred into potential energy, by jumping up. The resulting vault has for an increasing take-off angle, a faster increase of potential energy, a lower upward kinetic energy at the end of the vault and a shorter vault. The amount of energy stored in the pole decreases. 3100 Joules is the maximum amount of energy stored in the pole for the smallest angle of 3 degrees. The maximum amount of energy in the pole for the biggest angle (20 degrees) is 1300 Joules.

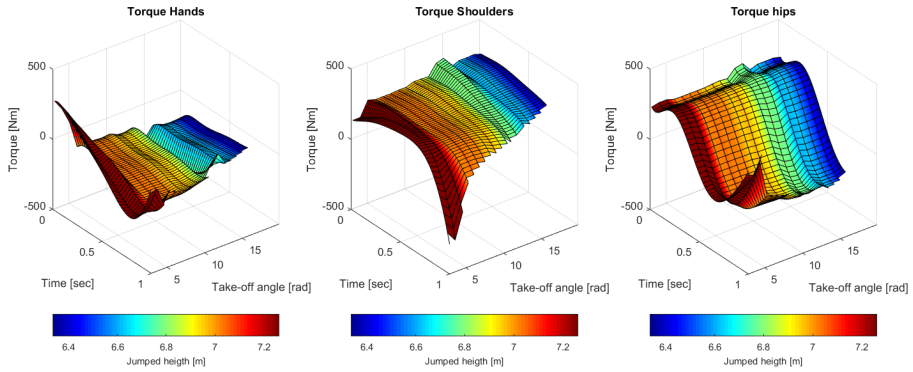

Figure 22: Optimized control torque profiles for the varied take-off angle over a range of 3 degrees up to 20 degrees. On the left: the torque applied at the tip of the pole. In the middle: the torque applied at the shoulders. On the right: the torque applied at the hips. Note: the color represents the jumped height. The maximum height is 7.26 meters, the minimum height of 6.33 meters is found at the biggest angle of 20 degrees.

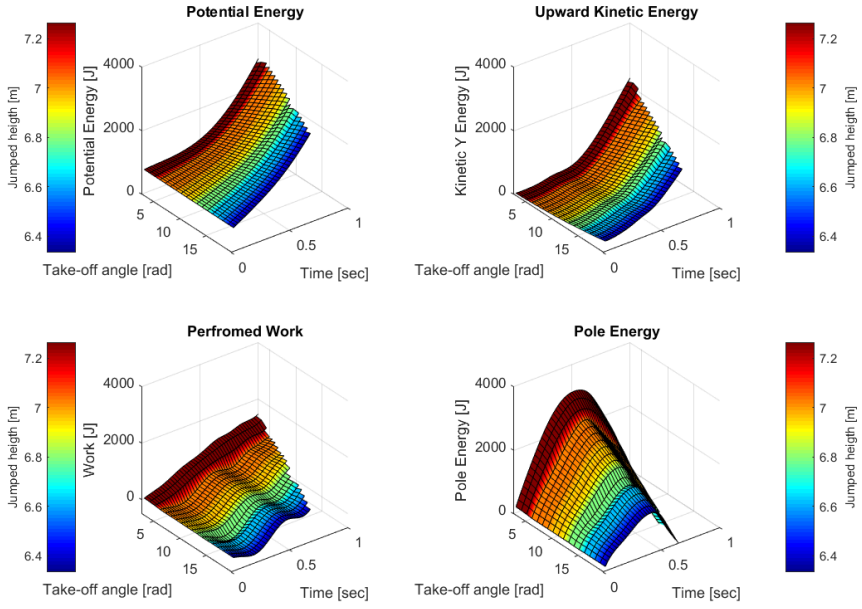

Figure 23: The amount of energy of each main energy component: potential energy at the top left, upward kinetic energy at the top right, the amount of performed work at the bottom left and the amount of energy stored in the pole at the bottom right. The difference in height is a result of a higher amount of upward kinetic energy. The maximum amount of energy stored in the pole increases for stiffer poles. The vaulted height is indicated by the color. The performance varies from 6 meters up to 7.4 meters.

Conclusion

The goal of this research was to provide the optimization of the control strategy of a simplified biomechanical model. With a sensitivity analysis, the influence of the pole properties and the initial properties of the vaulter are investigated to determine whether this is the cause of the different control strategies found by Brüggemann et al. [1999]. A sensitivity analysis of the take-off angle is investigated to determine the influence of the by Liu et al. [2011] suggested beneficial take-off angle at the pole plant.

Based on the found general trends and the different control strategies, the goal is fulfilled.

The following general trends or optima are found:

- The stiffer the pole, the better the performance
- The optimal pole length for the benchmark vaulter is 4.545 meters
- The lighter the vaulter, the better the performance
- The shorter the vaulter, the better the performance
- The smaller the take-off angle, the better the performance

Three main control strategies are found which are visual distinguished. The first strategy is the 'Extension-strategy' with a characteristic leg or shoulder extension. The strategy is found when the applicable torque is not high enough to point the feet up during the vault. This was the case with an increased mass, an increased length of the athlete and a decreased stiffness.

A second control strategy is found, called the 'Flexion-strategy'. The vault is not consistently found. Characteristic for this strategy is the lack of shoulder and hip extension. The arms are almost aligned with the trunk and the hip has an angle around 90 degrees at the moment of pole release.

The last control strategy is the 'Upwards strategy', Characteristic for this strategy is the small shoulder flexion, combined with a big hip extension. As a result, the feet point upwards at pole release.

Within the 'Upwards strategy', there are two power management strategies found. The first strategy is the 'Two Peaks' power strategy, the second power strategy is called 'Three Peaks'. Both strategies are shown in figure 8. The 'Two Peaks' strategy slowly merges into the 'Three peaks' strategy when the pole stiffness increased.

A clear difference of control is shown in by the 'Two Peaks' and 'Three Peaks' power strategy. A clear difference in motion between the two strategies is not found. This confirms the finding of Brüggemann et al. [1999]. Multiple control strategies are possible to for different sets of initial conditions and initial properties to maximize the vaulting performance.

Limitations and Recommendations

Optimization problems

The optimizer has a hard time with converging to a feasible minimum. The optimization procedure finds only around 40% of each try a minimum. The other 60%, the optimizer converges to an infeasible point.

The infeasbile solutions can be sorted out manually, resulting in only feasible vaults. The difference of the objective of the infeasible found solution is mostly around 4% of the maximal objective. Form an exploratory point of view, these difference are acceptable to find the global changes in control strategy between two different vaults and vaulters.

A possible reason for the bad convergence is caused by a combination of two factors. The first factor is the discretisation of the equations of motion. The second factor is the stopping cirterion where the pole is maximal 97% stretched. In the final stage of the optimization, the best solution is often one where the last step of the motion is very close to the edge of a 97% stretched pole. Such points are a very local optimum due to its advantage in potential energy. If the last time step of the motion is at a height of 95% of a stretched pole, then the amount of potential energy in the objective decreases with around 65 Joules for the bench mark pole of 4.57 meters. If the optimizer is in the feasible domain at a height close to 97% of the stretched pole, the optimizer decreases its step size, trying to increase the objective close to its current position. It will stop when the step size is below the step size tolerance. If the optimizer is not in the feasible domain, the optimizer searches for feasible solutions nearby, while maintaining the value of its objective. But due to its very local optimum, the next step will lower the objective. Often, the optimizer sticks to its current infeasible solution, decreases its step size, trying to get in a feasible domain close to its current position. Again, it will stop when the step size is below the step size tolerance.

The numerical integration step size of 0.02 seconds is a cause of not being able to step out of such a local optimum. With a smaller numerical integration step size, the surrounding solutions of the local minimum come closer. The optimizer is tempted to take a step from its local infeasbile optimum to a feasible solution, without lowering the objective.

The seven terms of equation B.7 are also picked arbitrarily and could be a cause of the slow convergence. Since there are 21 parameters to tweak, the optimizer has very many options to.

The initial guess is also an arbitrary factor in the optimization procedure. To investigate its influence, the optimization over the entire stiffness range is done a second

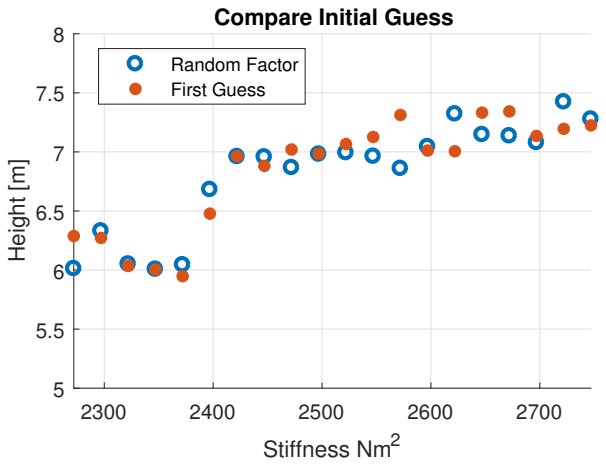

Figure 24: The final vaulted height is shown as a function of the pole stiffness in Nm^2. The vaulted heights are found with the first initial guess and with an intial guess by a random factor between 0.6 and 1.4. The biggest deviation is around 0.38 centimeters for a stiffness of $B = 2572\ Nm^2$, which is close to the a 6 % deviation.

time. However, this time, the initial guess is multiplied with a factor between 0.6 and 1.4. The resulting objectives of the first and the second optimization are shown in figure 24.

Vaulter Assumptions

The translation from the physiology of the vaulter to a simplified biomechanical model goes hand in hand with assumptions. The assumptions made by designing this model has to be considered when interpreting the results.

The most influential assumption of the presented model are the bounds on the energy sources of the model, the bounds on the control torques. Both the absolute bounds on the magnitude of the control torques, as well as the power bound, are both debatable.

The absolute bounds on the magnitude are found in McGinnis [1989] which used the bounds for a two dimensional forward dynamical model of the pole vault motion. The magnitudes are based on measurements performed on elite pole vaulters. However, the number of segments of the model McGinnis [1989] build was five, the hands were attached in a different manner, and simple muscle dynamics where implemented. There is not compensated for the difference between McGinnis' model and the presented model.

However, a control torque function with advanced muscle dynamical properties incorporated is also not suitable. It does not fit the purpose of the current model. A question which may arise is: How applicable is an advanced muscle dynamical model in a two dimensional biomechaincal model? A basic torque function per joint, dependent on the angular position and angular velocity is therefore recommended to increase the reliability while keeping the purpose of the model the same.

The maximal amount of power is supported by a basic trial and error analysis, as described in the Constraints section. The influence of the power constraint is shown in figure 3. Clearly, the power constraint blocks vaults from improving and forces the vaulter to change its power management strategy. As suggested above, a basic torque function per joint could be a step ahead to improve the model. By making the torque dependent on the angular velocity in combination with a power bound prevent the combination of a high torque and a high angular velocity.

Model Assumptions

The simplifications regarding the motion of the vaulter also comes at expense of the reliability of the model.

The two dimensional resemblance of the pole vault movement seems accurate during the majority of the pole support phase. Besides that, it makes the vault more applicable for an optimization due to the reduced number of degrees of freedom. However, in the final stage of the pole support phase, the vaulter turns the pole to the outside to not jump into it. The ability to apply a torque at the tip of the pole during and after this transition is questionable. The hand torque of the forward dynamical model McGinnis [1989] made is set to zero after 60% of the vault is completed. On the other hand, Morlier and Mesnard [2007] measured torques located at the tip of the pole up to 200 Nm.

The constraint of the presented model is a combined approach of Morlier and Mesnard [2007]. When the vault is completed for 50%, the absolute torque bound decreases from 600 Nm, found by McGinnis [1989], to 100 Nm at the end of the vault. As shown in figure 25, the influence of the constraint is only present at the end of the vault. Although there is no scientific support for the exact formulation of this constraint, it prevents the vaulter from producing unrealistic torque magnitudes for the position over the last 25% of the vault. The constraint seems therefore justified. The three segmental representation of the vaulter covers the main movements of the pole vault motion. Nevertheless, introducing more segments could result in more strategies, since there is an extra degree of freedom. Besides that, it could result in a shift of the range where the current strategies are found. Introducing a knee joint, for instance, changes the inertia and the location of the segmental center of mass. Less torque is needed to move the body in a more optimal position. A strategy which requires a high hip torque due to a high inertia of the legs is with a knee joint applicable for a wider range of initial parameters.

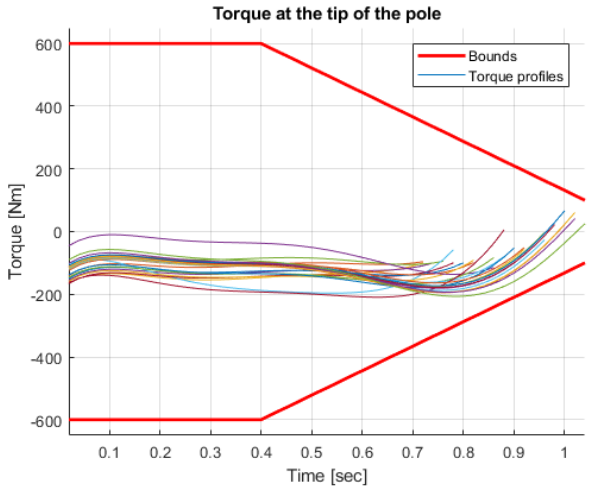

Figure 25: Control torque profiles for the entire range of the pole length. The bounds keep the magnitude of the torque within a feasible reagion. Note: the shown bound is only applicable for the longest torque profile in time. The constraint on the tip of the pole is dependent on the duration of the vault

The exclusion of the fly-away phase gives the current model the possibility to end in unrealistic positions and velocities. The feasible domain at the end of the vault is beyond realistic. The final positions have often almost no forward velocity, which makes crossing the bar in reality very difficult. The size of the feasible domain can be solved by introducing extra constraints at the end of the vault to guide the optimizer to a favourable final position. What this favourable position should look like, is not found in scientific literature. Besides that, the adaptability of the vaulter at the end of the vault is hard to estimate. Therefore, an extension of the current model is suggested where a true pole release phase and fly-away phase is simulated to ensure feasible vaults.

A reduced feasible domain at the end of the vault can also reduce the sensitivity of the initial guess, because there is a smaller region to converge to. Even though the variation between the final objective stays below 5%, it is still not said that the global optimum is found for a given set of initial conditions and initial properties.

References

G.P. Brüggemann, D. Koszewski, and H. Müller. *Biomechanical Research Project: Athens 1997: Final Report: Report on the Biomechanical Research Project at the 6th World Championships in Athletics, Athens 1997, Sponsored by the International Athletic Foundation*. Meyer und Meyer Sport, 1999.

H Adamczewski and Bettins Perlt. Run-up velocities of female and male pole vaulting and some technical aspects of women's pole vault. *New studies in athletics*, 12:63–76, 1997.

Nebojša Zagorac, Edvard Retelj, and Ratko Katić. Successful pole vault influenced by certain kinematical parameters. *Collegium antropologicum*, 32(4):1133–1139, 2008.

Nicholas P Linthorne and AH Gemma Weetman. Effects of run-up velocity on performance, kinematics, and energy exchanges in the pole vault. *Journal of sports science & medicine*, 11(2): 245, 2012.

Guangyu Liu, Sing-Kiong Nguang, and Yanxin Zhang. Pole vault performance for anthropometric variability via a dynamical optimal control model. *Journal of Biomechanics*, 44(3):436–441, 2011.

Nicholas P Linthorne. Energy loss in the pole vault take-off and the advantage of the flexible pole. *Sports Engineering*, 3(4):205–218, 2000.

Nicholas P Linthorne, Maurice S Guzman, and Lisa A Bridgett. Optimum take-off angle in the long jump. *Journal of sports sciences*, 23(7):703–712, 2005.

Julien Frère, Beat Göpfert, Jean Slawinski, and Claire Tourny-Chollet. Effect of the upper limbs muscles activity on the mechanical energy gain in pole vaulting. *Journal of electromyography and kinesiology*, 22(2):207–214, 2012a.

Marco M. Reijne. The next level in pole vaulting. Master's thesis, Delft University of Technology, 5 2016.

Julien Morlier and Mariano Cid. Three-dimensional analysis of the angular momentum of a pole-vaulter. *Journal of biomechanics*, 29(8):1085–1090, 1996.

Falk Schade, Adamantios Arampatzis, and Gert-Peter Brüggemann. Influence of different approaches for calculating the athlete's mechanical energy on energetic parameters in the pole vault. *Journal of Biomechanics*, 33(10):1263–1268, 2000.

AL Schwab and M Wisse. Basin of attraction of the simplest walking model. In *Proceedings of the ASME design engineering technical conference*, volume 6, pages 531–539, 2001.

Mats Ekevad and Bengt Lundberg. Simulation of 'smart' pole vaulting. *Journal of Biomechanics*, 28(9):1079–1090, 1995.

Jason K Moore, Mont Hubbard, JDG Kooijman, and AL Schwab. A method for estimating physical properties of a combined bicycle and rider. In *ASME 2009 international design engineering technical conferences and computers and information in engineering conference*, pages 2011–2020. American Society of Mechanical Engineers, 2009.

Mont Hubbard. Dynamics of the pole vault. *Journal of Biomechanics*, 13(11):965–976, 1980.

Julien Frère, Beat Göpfert, François Hug, Jean Slawinski, and Claire Tourny-Chollet. Catapult effect in pole vaulting: Is muscle coordination determinant? *Journal of electromyography and kinesiology*, 22(1):145–152, 2012b.

Julien Morlier and Michel Mesnard. Influence of the moment exerted by the athlete on the pole in pole-vaulting performance. *Journal of biomechanics*, 40(10):2261–2267, 2007.

Peter M McGinnis. Pete's pointers for perfect pole vaulting. *Track Technique*, 109:3472–3474, 1989.

AL Schwab and RQ van der Linde. Multibody dynamics b, 1997.

William E Boyce, Richard C DiPrima, and Douglas B Meade. *Elementary differential equations and boundary value problems*, volume 9. Wiley New York, 1992.

Appendix A Matlab Model

The complete MATLAB optimization program is built on two functions and the optimizer `fmincon`. MATLAB is used since the script of Reijne [2016] was also built in MATLAB. The function `fmincon` is used since the optimization problem is a constrained, multi variable problem. It fits the best to the optimization problem.

The goal of the optimization is to maximize the sum of potential and upward kinetic energy by optimizing the control torques at the hand, shoulder and hip. This is also described in section Objective. The control torques are optimized by changing the parameters A to G of the polynomial:

$$T_c(t) = At^6 + Bt^5 + Ct^4 + Dt^3 + Et^2 + Ft + G \quad \text{(A.1)}$$

Each hinge needs its own torque profile, so each torque profile has its own set of torque parameters. This gives 21 parameters to optimize. In Matlab, the torque functions and the set of torque parameters are numbered where `T1_fun` is the torque located at the tip of the pole, `T2_fun` is the torque actuator located at the shoulders and `T3_fun` is the torque actuator located at the hips as shown in figure A.1. The torque parameters are stored in vectors called `INP_T1_fun`, `INP_T2_fun` and `INP_T3_fun`.

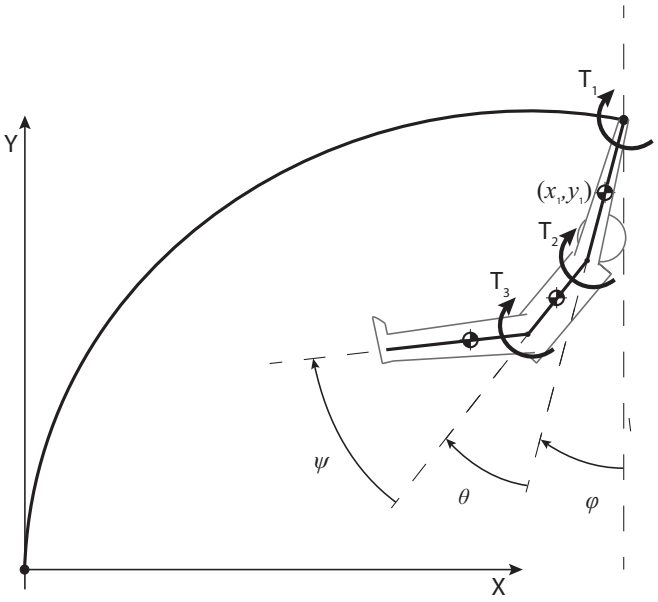

Figure A.1: Simplified model representation. Generalized coordinates: the center of mass of the arms (x, y), the angle at the hands (ϕ), the angle at the shoulders (θ) and the angle at the hips (ψ). Control torques: T_1 is located at the top of the pole, T_2 is located at the shoulders, T_3 is located at the hips

The development of the optimization model started with spline functions as torque profiles. How the spline function works is explained in section Initial guess. In that stadium of development, the spline functions often did not find an optimum. On advice of T. Geijtenbeek, postdoctoral researcher at Biomechanical Design, the switch was made to polynomials to get more flexibility in the final torque profile. A 6^{th} degree polynomial gave a very accurate fit to the spline function, with a root mean square error of 0.99. The optimization time turned out to be in the order of hours which is not excessively long. So, the current polynomial is chosen to be the function to optimize.

The Script

The optimization is started from the main file `Optimization.m`. The file contains two functions besides a call to `fmincon`:

- The objective function, to calculate the amount of energy for a given set of input variables
- The constraint function, to check whether all the variables fulfill the constraints

The first part of `Optimization.m` is the design set-up. In this part, the properties of the pole (length and stiffness), vaulter (mass, length, inertia) and other optimization parameters (integration time step size, pole discretization) are determined. These variables are written in the vector `INP_ode`. In the second part of `Optimization.m`, the initial position and velocities of the generalized coordinates, shown in figure A.1, are calculated.

Initial position

Several initial parameters are varied and optimization to find the influence on the vaulter's control strategy. The variations have influence on the amount of energy the vaulter starts with. If the stiffness or the length of the pole is

changed but the position of the tip stays the same, the vaulter starts each optimization with a different amount of initial pole energy.
A choice has to be made to keep the initial energy the same when, for example, the pole length is varied. The following energy balance should be constant:

$$E_{vaulter} + E_{pole} = \left[E_k + E_p\right] + E_{pole} = \left[\frac{1}{2}mv^2 + mgh_{com}\right] + \frac{1}{2}B\kappa^2 = C \tag{A.2}$$

Where the energy of the vaulter is split into potential energy, E_p, and kinetic energy, E_k. Both the kinetic energy and potential energy are calculated with respect to center of mass of the vaulter. The energy of the pole is a function of stiffness B and $kappa$, where,

$$r = \frac{1}{\kappa} \tag{A.3}$$

Assumed that the pole is curved as a perfect circular arc, radius r is solved from the relation of the length of the pole chord and the length of the pole:

$$\sin\left(\frac{L_{pole}}{2r}\right) = \frac{L_{chord}}{2r} \tag{A.4}$$

C is set equal to what Brüggemann et al. [1999] found by the elite vaulters at the World Championships of 1998. The sum of potential and kinetic energy per kilogram body weight was 57.03 Joules per kilogram body weight. The amount of potential energy is calculated according to the bench mark position of table 1. The remaining part of initial energy is kinetic energy and corresponds to a velocity of 9.7 m/s. This is measured at the last stride before the pole is planted and the vaulter takes off. During the pole plant and take-off, the vaulter looses around 10% of his energy. The resulting energy is 51.327 Joules per kilogram body weight.

If the position of the tip of the pole stays the same but the pole length increases, the curvature of the pole should increases, resulting in more pole energy. The velocity of the vaulter is reduced to fulfill the energy balance in equation A.2. As shown in figure A.2, the velocity does not changes drastically.

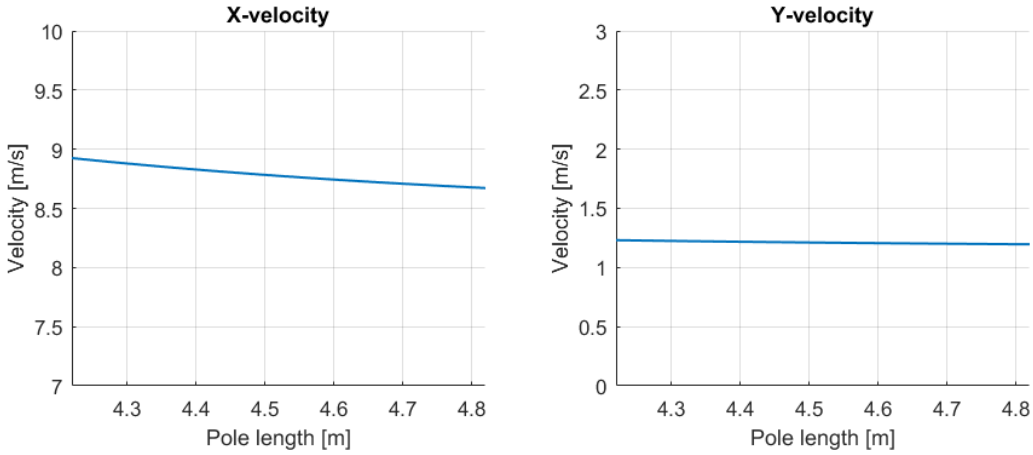

Figure A.2: On the left: the change of velocity of the vaulter in x-direction when the velocity is adjusted to fulfill the energy balance of equation A.2. On the right: the change of velocity of the vaulter in y-direction when the velocity is adjusted to fulfill the energy balance of equation A.2.

If the curvature stays the same, the position of the tip has to change if the pole length increases. Keeping the position constant lead to a small curvature when the pole length decreases. The pole reaction forces for a small curvature are much higher for the absolute torque bounds at the tip of the pole, as shown in figure A.3. To avoid high pole forces, the position of the tip of the pole is changed to fulfill the energy balance.

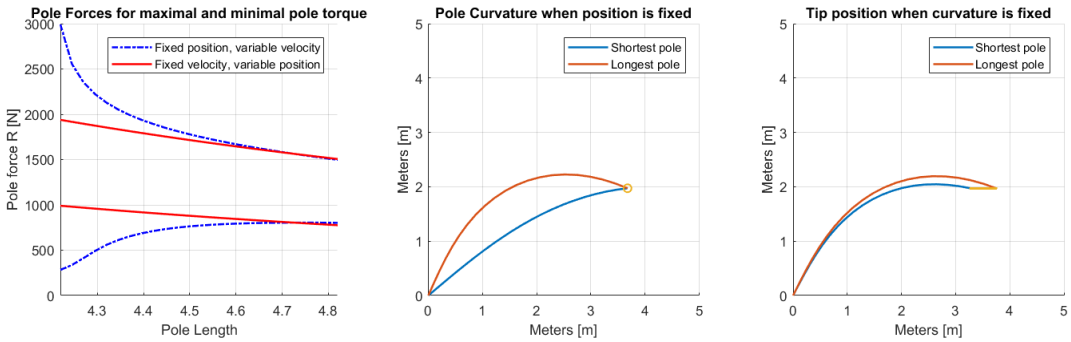

Figure A.3: On the left: the maximal and minimal pole forces at the start of the optimization for different pole length. The velocity of the vaulter or the position of the tip of the pole is changed to fulfill the energy balance of equation A.2. Varying the initial position results in lower pole forces which is preferred in the optimization. In the middle: the curvature of the shortest and longest pole used in the optimization when the velocity is varied to fulfill the energy balance of equation A.2. On the right: the shift of the tip of the pole when the pole length is varied but the curvature stays the same.

The approach described above is also used when the stiffness is varied. Varying the mass of the athlete increases the potential energy. This is covered by reducing the velocity while keeping the direction of the velocity, or take-off angle, the same. When the length is varied, the amount of potential energy increases which is covered by reducing the velocity. Again, by keeping the direction of the velocity the same. The position of the tip of the pole also shifts slightly along the circle with the pole chord as radius.

Objective function

The objective function calculates each iteration, the sum of potential and upward kinetic energy during the entire vault, as a function of the torque parameters (see paper section Objective). The maximum of the sum is taken as the moment the vaulter releases the pole. The input variables are the torque parameters, the time step size of the numerical integration, the initial conditions (`X_ode`) and the initial parameters (`INP_ode`). The objective function is in essence the same as the model M. Reijne. It is adjusted for optimization of the control torques. The vaulter contains three segments instead of two, and an inertia model is introduced.

First, the objective processes the input vectors into separate input variables. The variables are used in a for-loop which calculates the movement according to the input. The loop stops if the pole is stretched for 97% or the pole force equations, described below, cannot be solved. The loop stops before the pole is fully stretched. The solver which calculates the pole forces cannot cope with a almost fully stretched pole.

Pole forces

The loop starts by calculating the shape of the pole and the force of the pole acting on the vaulter. The shape is given by the angle γ, shown in figure A.4
The angle γ is defined as the angle between the tangent of the pole, located at the origin, and the line parallel to R, crossing the origin. The pole force is denoted as R. R and γ are found by the function `myfun` which is built by M. Reijne. The input variables of `myfun` are the length and stiffness of the pole, the length of the pole chord and the torque at the tip of the pole.

The solver `fsolve` is used to solve the set of equations of `myfun`. To do so, `fsolve` needs an initial guess. The first initial guess is based on trial and error and stored in the vector `INP_ode`. An accurate initial guess will decrease the computational time. For the next time step, the previous solution is used as an initial guess, since γ and R change gradually during a simulated vault as shown in figure A.5.
If the found R and γ are both positive, the for-loop continues. If γ is negative, the pole has a convex shape from the vaulter's point of view which is impossible to have. If R is negative, the pole pulls on the vaulter towards the origin, which is also impossible for a realistic vault. So, if one of these situations occurs, the simulation stops.

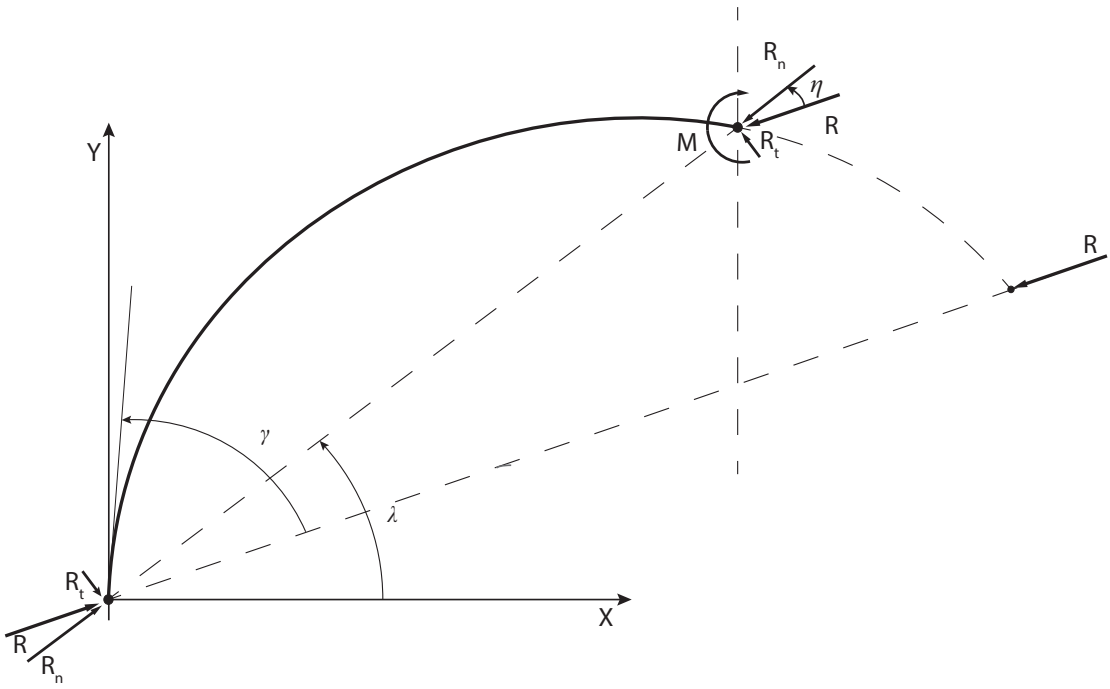

Figure A.4: The pole force and pole shape is determined by pole force R and angle γ, located between the tangent at the origin and the line parallel to R, crossing the origin. The angle λ is the angle between the pole chord and the x-axes. The angle η is calculated with the elliptic integrals to find the pole forces R_n and R_t

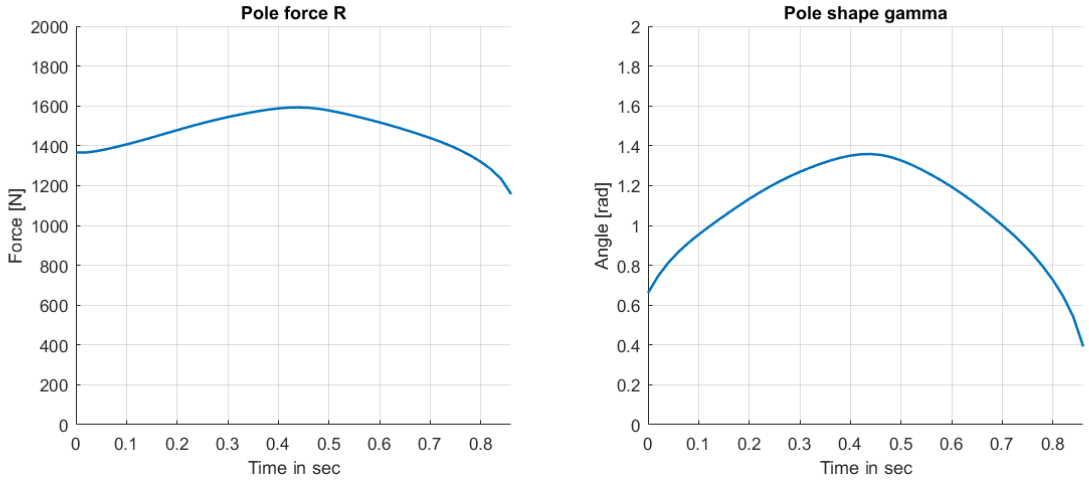

Figure A.5: An example of the pole force and pole tangent γ during a vault. Both graphs develop very gradual

Besides R and γ, the solver gives an exit flag as output. If the exit flag is not equal to one, which is given when a solution is found, the simulation stops. Otherwise, `fsolve` has found a valid R and γ and the for-loop continues. The old values of R and γ are overwritten in `INP_ode` as a new initial guess.

Equation of Motion

The function of the equation of motion is used, called `odefun`. The derivation of the equation of motion is found in Appendix - Equations of motion. The output of the function are the velocities and accelerations of the generalized coordinates for the next time step as a function of the current position, velocities and torques.

`Odefun` has multiple input variables. The first input variable is the moment in time, `t`. The second input variable is the vector `X_ode` which contains the position and velocities of the generalized coordinates at the start of the time step. The next three input vectors are the optimization variables parameters A to G. The last input vector is `INP_ode`, containing the properties of the vaulter, the pole properties, R, γ and the gravitational constant.

The inertia of each segment with respect to the center of mass of the vaulter, is needed to use the equation of motion. Every time `odefun` is used, the inertia is calculated since the position of the vaulter changes and the inertia changes with the position of the vaulter. The amount of torque of each actuator is calculated by its own function called `T1_fun`, `T2_fun` and `T3_fun`. The function and its input is shown in equation A.1.

The values of the generalized positions and velocities, together with the pole forces and control torques are filled in into the matrices and vectors needed for the TMT-method. The result is a reduced mass matrix and an extended force vector (Appendix - Equations of motion). The system is solved using the backslash operator. The resulting vector contains the accelerations of the current situation. The output vector of `odefun.m` contains, besides the found generalized accelerations, the generalized velocities.

The equations of motion are numerically solved by the 4th order Runge-Kutta scheme, explained in Appendix - Numerical integration. The function calculates for four situations the velocities and the accelerations of the equations of motion and takes a weighted average of these four situations as the of the equation of motion. To solve the equations of motion, the pole force `R` is needed. Since the amount of torque is time dependent, the function `fsolve` is used again to calculate the pole forces for the four situations the RK4 scheme needs. The setup of `fsolve` and `myfun` is the same as described above. The only thing which is adjusted is the initial guess of R and γ as they are overwritten in `objective.m`. The force R is with elliptic variables transformed into forces R_t and R_n which are defined in the pole coordinate system, as shown in figure A.4. If `fsolve` does not find a solution, as described above, the simulation stops.

The equations of motion provide the velocities and accelerations for every time step. With numerical integration, the next position and velocities can be calculated. The numerical integration scheme, explained in Appendix - Numerical integration, is written as a function with all the input the equations of motion need. The output is the position and velocities of the generalized coordinates at the next time step. The function calculates for four situations the velocities and the accelerations of the equations of motion. If one of the situations does not result in a solution due to `fsolve`, the output the entire integration step is set to zero. If each step results in a solution, then the next step in time is calculated and returned to `objective.m`. The solution of the numerical integration is stored in a vector per generalized coordinate and generalized velocity. Matlab breaks the for-loop if the entire output vector of the numerical integration is zero which means the pole is almost stretched, or `fsolve` could not solve the problem. Based on the experience with the model, the inability of `fsolve` to find a solution mainly occurs with unsuccessful vaults with an unrealistic combination of pole shape and pole forces.

When the for-loop ends, the trajectory and velocity of each segment is calculated. The potential energy and upwards kinetic energy are calculated for the entire vault. The potential energy is calculated as the sum of the potential energy of each segment. The same goes for the upward kinetic energy. Note that in the script, the sum of these two parameters is denoted as a negative value since `fmincon` searches for a minimum. So, the output of `objective.m` is the minimum value of these two parameters. The moment in time and the final value of the objective function is found with the `min` command in Matlab. Every set of torque inputs `fmincon` tries is stored in

a matrix to analyze the search of `fmincon` if necessary.

Contraint function

The constraint function, `nonlcon.m`, is the second vital function `fmincon` needs to function properly. This function determines the design space by putting bounds on variables. The bounds are formulated as inequality constraints where a value below zero means the constraint is fulfilled.

The constraint on the highest point of the vault for instance, explained in section Final position, is formulated as:

$$c_1 = x_{final} \leq 0$$

$$c_2 = -x_{final} - 0.8 \leq 0$$

In this way, the value of x_{final} will be between 0 and 0.8 which is the region the vaulter may place the bar.

The first constraint in the constraint function is the length of the pole chord. The length of the pole chord should always be less than the length of the pole. The second constraint is the sign of γ. For a realistic shape, γ should always be negative, resulting in a concave shape. The maximal value of gamma should be below zero. The next four constraints are formulated so that no element will go through the ground. The seventh constraint makes sure the vault only ends when the pole is stretched for 97 percent of its unloaded length. The eighth and ninth constraint are the constraints for the final position and described in the example. The next six constraints are the bounds set for the joints, to overcome hyper flexing and hyper extension. Then, six constraints are the bounds which constraint the maximal and minimal amount of torque of each actuator. The last four constraints bound the amount of power at the shoulders and the hips, as explained in section Control.

The solver `fmincon` tries each iteration to fix the constraints which are violated the most. Besides that, `fmincon` sometimes takes steps slightly outside the region where all the constraints are fulfilled, to check if the objective can be improved. The constraints are normalized by their bound to make sure every constraint is equally important to solve and do not block improvements because of their magnitude.

If there are certain constraints that are more important, a penalty could be introduced to increase the magnitude of the constraint.

There is an option to constrain the 21 optimization parameters of the control torques, outside the constraint function in `Optimization.m`. Each parameter is then bounded by a certain magnitude. This option is not used since the shape of the control torques should not be constrained.

The constraint bounds are given in the script `Optimization.m`. The bounds are stored in the vector `INP_con` and is one of the input vectors for the constraint function. The other input vectors are the same as the objective function: the optimization variables for each torque function, the time step size, the initial position `X_ode` and system properties `INP_ode`. The constraint function is very similar to the objective function. The function starts with processing the input vectors into separate input vectors or input variables. Then, the same for-loop as the objective starts but, in this function, several variables are saved in a vector to check their magnitude during the entire vault. The magnitude of the torques and the length of the pole chord for instance.

The conditions to break out of the loop are the same as in the objective function. The loop stops when `fsolve` cannot find a proper solution for the shape of the pole. When the loop is finished, the trajectory and velocities of each element is calculated. The potential energy and upwards kinetic energy are calculated for the entire vault. The potential energy is calculated as the sum of the potential energy of each segment. The same goes for the upward kinetic energy. The moment in time and the final value of the maximal energy is found with the `max` command in

Matlab. All constraints are checked until the maximal amount of energy is reached. At that moment, the vaulter starts the fly-away phase which does not involve the pole.

The output of `nonlcon.m` are the answers of the constraint equations of each iteration. The results are saved in a separate matrix to see which constraints are broken during the optimization and which constraints make the vault infeasible.

Initial guess

The last input `fmincon` needs is a place to start the optimization, an initial guess. The initial guess determines the first shape of the torque functions. Picking an initial guess can make or break the optimization. A bad initial guess far from the optimum results in long computational times. An initial guess which breaks many constraints also results in long computational times or can even result in not finding an optimum at all. The initial guess is determined in a different script. The script is again very similar to the objective function. The same for-loop is used, resulting a trajectory based on the guessed torque function. The vault is visualized to see if the vaulter breaks the constraints.

The sixth-degree polynomial is hard to interpret by guessing the optimization parameters. So, a spline function is used instead to make a first estimation of the control torques. The shape of the spline function is made by fixing the value of the torque-function every tenth of a second. By fixing eleven points throughout the torque function, the magnitude, which preferably is below the constrained value, is much easier to estimate than a sixth-degree polynomial. These eleven points are the input of the `spline` command of Matlab which creates the torque functions as a function of time.

Now the new torque functions are made, the for-loop, described in section Objective of this chapter, is used to determine the final trajectory. Based on the visualization, it is easier to see where the torque is to high or to low. By trial and error, the eleven points in time, which determines the shape of the spline, are tweaked until a rough realistic vault is found.

The eleven points per torque function are translated into a sixth-degree polynomial using the curve fit application of Matlab. Now, the seven parameters per torque function are known and used as the initial guess for the check of the constraints.

The constraint check is performed in the same script as the entire optimization with one small adjustment, the objective function is set to zero. This results in a major change of behavior of `fmincon`. The optimizer now only moves in the direction were all the constraints are met. Two constraints are made stricter to leave room for the true optimization. These constraints describe the space where the highest point should be reached ref final position. When the initial guess breaks these constraints, it often results in a non-feasible outcome. After the constraint check is performed, an initial guess is found within the feasible domain which most likely gives a feasible optimum.

Optimization options

Now, all the input needed for an optimization are formulated. So, the `fmincon` function is formulated with the objective function, the initial guess, the parameter bounds, the constraint function and the solver options. The solver returns the resulting objective, the maximal amount of energy, and the 21 torque parameters, which results in the maximal amount of energy.

The `fmincon` function has several options to make the optimization fit to a specific problem. The most important option is selecting the algorithm `fmincon` uses to solve the problem. Each algorithm has its own strong and weak points. For the pole vault optimization, the Sequential Quadratic Programming, or SQP, is used. The algorithm is not the fastest algorithm of the other options, but it is very robust, meaning it can cope with complex interactions between reaching the objective and fulfilling the constraints.

The complexity of the constraints is the result of the causality of the optimization parameters and the different types of constraints. The torque constraints for instance are very straightforward. The maximal and minimal torque

at the tip of the pole are direct related to its seven optimized parameters. The constraints on the position however, are dependent on the combination of the three torque parameters and the torque's curve over time.

Another complexity of the combination of constraints is the difference in magnitude. The joint angles are expressed in radians. So, a violation of a joint angle constraint will be in the order of 10^{-3}. A violation of the torque bounds however, is often in the order of 10^{1}. Most algorithms use the magnitude of the violation as a measure of importance. Torque constraint violations are therefore completed in an earlier stage of the optimization then the joint angle constraints. The constraints are normalized by the magnitude of their bound to cope with the difference in importance.

The SQP algorithm has the option `Scale problem` which normalizes the constraint function and objective function. With this property switched on, the optimization is often able to stay close to the feasible domain. The downside is the slow convergence of the objective function which is shown in figure A.6. A self-written normalization of the constraints and a switch to the interior-point algorithm, which tend to converge faster, is a possible improvement.

Two optimization options are exit-bounds for the optimization procedure. The bounds are determined by a trial and error approach. The first bound is the maximal amount of function evaluations, this is the number of tries `fmincon` can use to find the optimum. It is currently set on 1500 function evaluations.

As described above, the convergence can take a long time. When a certain optimization takes 1500 function evaluations, the objective increases in general less than 3% over the second half of the optimization. The feasibility, the biggest constraint violation, is often in the order of 10^{-3} and decreasing. Since the constraints are normalized, the feasibility corresponds to a violation of 0.1%. Based on that, it can be concluded that the strategy does not change but improves slightly. 1500 function evaluations seem therefore sufficient. The convergence is shown in figure A.6. Here, the slow convergence at the end of the optimization is clearly visible.

The step size tolerance is the second option. The step size is a lower bound tolerance and is determined as the norm of the difference of the previous try and the current try. The step size is set to 10^{-6} to stop extreme slow convergence. If `fmincon` makes a step with a step size below the bound, it stops the optimization. Changing the step size tolerance is another way to increase the convergence speed. However, the SQP algorithm tend to take small steps at the beginning of the optimization. A too big step size tolerance can block these steps, forcing `fmincon` to stop. Therefore, a small step size tolerance is preferred.

The last option, which does not stop the optimization, is a tolerance on the constraints. The tolerance is currently set on 10^{-3}. As described above, a constraint violation with 0.1% is permitted. During the optimization, `fmincon` some times takes steps outside the feasible domain to increase the objective. By introducing a constraint tolerance, `fmincon` takes bigger steps outside the feasible domain in the direction of a better objective which makes the optimization faster. However, the risk of converging into a feasible domain is slightly bigger. The optimizer does not store his previous steps. If the step into the infeasible domain is to big, `fmincon` could start converging in this region, resulting in a failed optimization.

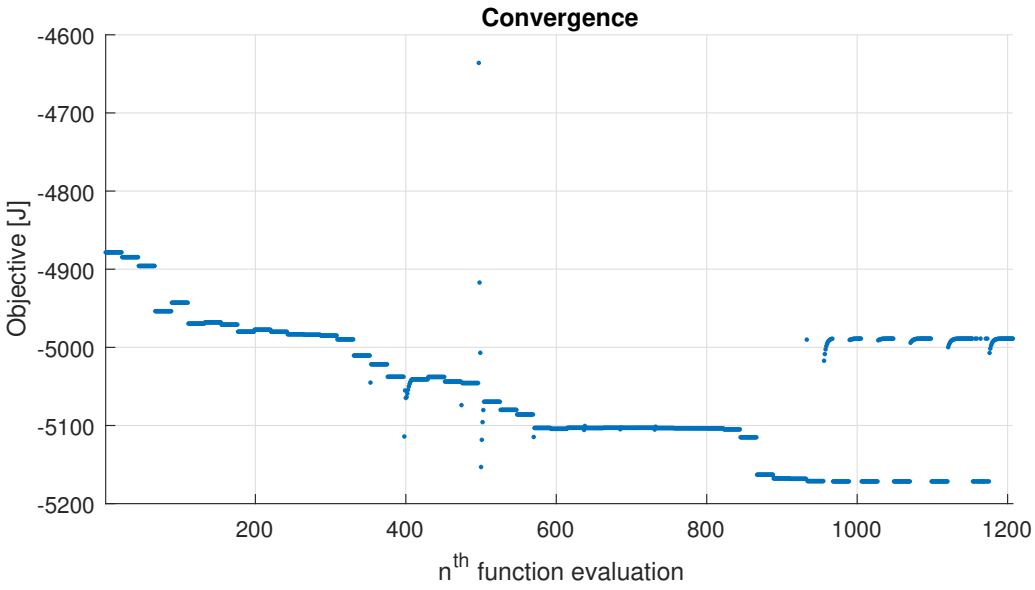

Figure A.6: A typical example of the development of the objective value. After 600 iterations, the objective converges slowly. The last 600 calculations calculations do not improve the vault significantly. A maximal amount of 1500 function evaluations seems therefore sufficient.

Appendix B Equations of motion

Multiple methods are available to calculate the equations of motion of a multi body system with each its own strength and flaws. The equations of motion for the optimization model are derived with the TMT-method, a combination of using generalized coordinates formulated by Lagrange, virtual power and inertia contribution via d'Alembert forces. The exact derivation how the Lagrange method and d'Alembert's principle are combined can be found in Schwab and Linde [1997].
The TMT-method is used since it is very computational efficient. This is a big plus. The equations of motion are evaluated over a hundred thousand times during a complete optimization.

General Approach

The equations of motion are based on a set generalized coordinates (q). This is a set of independent variables which describe the position and orientation of each body of a multi-body system. There is no recipe to determine generalized coordinates.

The final form of the equations of motion is given by equation (B.1) and contains five elements:

$$T_{i,k} M_{ij} T_{j,l} \ddot{q}_l = T_{i,k} \sum f_i + T_{i,k} M_{ij} h_j \tag{B.1}$$

The first element is the kinematic transformation matrix T. It is the geometric relations between the generalized coordinates and the x-position, the y-position and orientation of each body, derived with respect to q. The chosen set of generalized coordinates keeps the kinematic transformation compact.

The second element is the mass matrix M which contains the mass and inertia per body on the diagonal. The third element is the second derivative of the generalized coordinates with respect to time, $\ddot{q}$. The fourth element is the vector containing the sum of the forces of each body, f. The final element is h which contains the convective accelerations, a component of the time derivation of the transformation matrix.

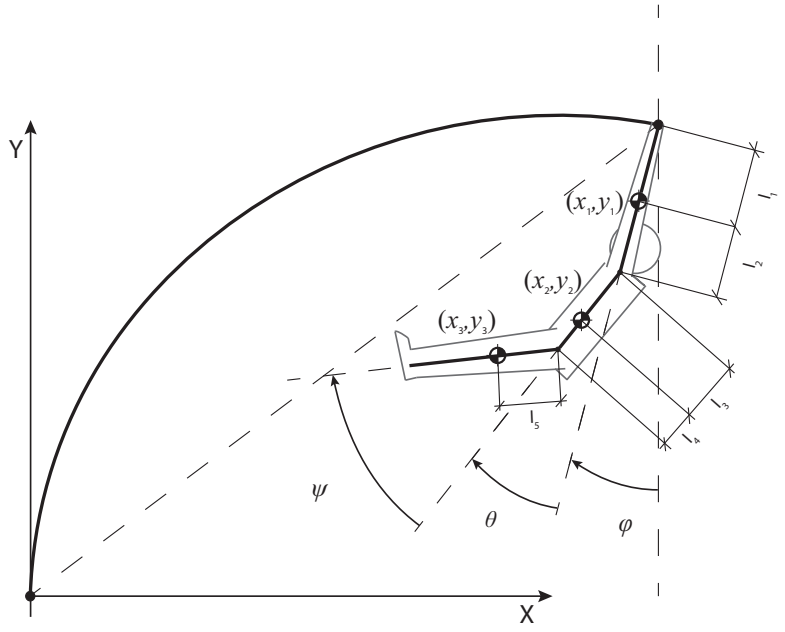

Figure B.1: Simplified model representation with generalized coordinates: the center of mass of the arms (x, y), the angle at the hands (φ), the angle at the shoulders (θ) and the angle at the hips (ψ). Distances l_1, l_2, l_3, l_4 and l_5 locate the center of mass of each body.

Derivation

The general setup, as described above, is now applied to the model shown in figure B.1. Here, the positions of the center of mass is shown, together with the joint angles ϕ, θ and ψ and the distances l_1, l_2, l_3, l_4 and l_5 which determine the location of the centers of mass of each body and the tip of the pole.

Positions

The body of the vaulter is modelled as of three bodies with each three degrees of freedom, the x-position, the y-position and an orientation angle.

$$x_i = \begin{bmatrix} x_{cm1} \\ y_{cm1} \\ \phi \\ x_{cm2} \\ y_{cm2} \\ \phi+\theta \\ x_{cm3} \\ y_{cm3} \\ \phi+\theta+\psi \end{bmatrix} \tag{B.2}$$

The mass matrix corresponding to the notation of x_i is:

$$M_{i,i} = \begin{bmatrix} m_1 & & & 0 & & & 0 \\ & m_1 & & & & & \\ & & I_1 & & & 0 & \\ & & & m_2 & & & \\ 0 & & & & m_2 & & 0 \\ & & & & & I_2 & \\ & & 0 & & & & m_3 \\ & & & & & & & m_3 \\ 0 & & & 0 & & & & I_3 \end{bmatrix} \tag{B.3}$$

The set of degrees of freedom can be described using five generalized coordinates, the x and y position of body one, the arms, the angle ϕ, the angle θ and the angle ψ. These five variables are the generalized coordinates, stored in q_j.

$$q_j = \begin{bmatrix} x_{cm1} \\ y_{cm1} \\ \phi \\ \theta \\ \psi \end{bmatrix} \tag{B.4}$$

The geometric relations of x_i as a function of q_j are given by:

$$g_i = \begin{bmatrix} x_{cm1} \\ y_{cm1} \\ \phi \\ x_{cm1} - l_1 sin(\phi) - l_3 sin(\phi+\theta) \\ y_{cm1} - l_1 cos(\phi) - l_3 cos(\phi+\theta) \\ \phi+\theta \\ x_{cm2} - l_4 sin(\phi+\theta) - l_5 sin(\phi+\theta+\psi) \\ y_{cm2} - l_4 cos(\phi+\theta) - l_5 cos(\phi+\theta+\psi) \\ \phi+\theta+\psi \end{bmatrix} \tag{B.5}$$

Now, the positions can be described with only five generalized coordinates, stored in q_j.

Velocities

The linear and angular velocities of x as a function of the velocities of q are found by taking the derivative of x with respect to time. This results in two factors because of the chain rule.

$$\dot{x}_i = T_{ik}\dot{q}_k \tag{B.6}$$

The first term is transformation matrix T which is g_i derived with respect to q_j. The second term is q_j derived with respect to time, resulting in $\dot{q}$.

$$T_{i,k} = \begin{bmatrix} 1 & 0 & 0 & 0 & 0 \\ 0 & 1 & 0 & 0 & 0 \\ 0 & 0 & 1 & 0 & 0 \\ 1 & 0 & -l_2 cos(\phi) - l_3 cos(\phi+\theta) & -l_3 cos(\phi+\theta) & 0 \\ 0 & 1 & l_2 sin(\phi) + l_3 sin(\phi+\theta) & l_3 sin(\phi+\theta) & 0 \\ 0 & 0 & 1 & 1 & 0 \\ 1 & 0 & -l_2 cos(\phi) - (l_3+l_4) cos(\phi+\theta) - l_5 cos(\phi+\theta+\psi) & -(l_3+l_4) cos(\phi+\theta) - l_5 cos(\phi+\theta+\psi) & -l_5 cos(\phi+\theta+\psi) \\ 0 & 1 & l_2 sin(\phi) + (l_3+l_4) sin(\phi+\theta) + l_5 sin(\phi+\theta+\psi) & (l_3+l_4) sin(\phi+\theta) + l_5 sin(\phi+\theta+\psi) & l_5 sin(\phi+\theta+\psi) \\ 0 & 0 & 1 & 1 & 1 \end{bmatrix} \tag{B.7}$$

The multiplication of these two terms gives the linear and angular velocity of every body as a function of q_j and $\dot{q}$.

Accelerations

The transformation of the accelerations of q_j into the accelerations of x is done in the same manner, by taking the time derivative of the velocities $\dot{x}$.

$$\ddot{x}_i = \frac{\partial g_i}{\partial q_l}\ddot{q}_l + \frac{\partial^2 g_i}{\partial q_m \partial q_p}\dot{q_m}\dot{q_p} \tag{B.8}$$

This equation consists of two terms each containing two factors, as a result of the chain rule. The first term is nothing more than $T_{i,k}$ multiplied by the generalized accelerations. The second term is called the convective accelerations, further denoted with h. The vector h is found by taking the derivative of the T with respect to q. The resulting vector h is:

$$h = \begin{bmatrix} 0 \\ 0 \\ 0 \\ h_4 \\ h_5 \\ 0 \\ h_7 \\ h_8 \\ 0 \end{bmatrix} \tag{B.9}$$

With:

$$h_4 = l_2\dot{\phi}^2 sin(\phi) + l_3\dot{\phi}^2 sin(\phi+\theta) + l_3\dot{\theta}^2 sin(\phi+\theta) + 2l_3\dot{\phi}\dot{\theta} sin(\phi+\theta) \tag{B.10}$$

$$h_5 = l_2\dot{\phi}^2 cos(\phi) + l_3\dot{\phi}^2 cos(\phi+\theta) + l_3\dot{\theta}^2 cos(\phi+\theta) + 2l_3\dot{\phi}\dot{\theta} cos(\phi+\theta) \tag{B.11}$$

$$
\begin{aligned}
h_7 = l_2\dot{\phi}^2 sin(\phi) + l_3\dot{\phi}^2 sin(\phi+\theta) + l_3\dot{\theta}^2 sin(\phi+\theta) + 2l_3\dot{\phi}\dot{\theta} sin(\phi+\theta) + \\
l_4\dot{\phi}^2 sin(\phi+\theta) + l_4\dot{\theta}^2 sin(\phi+\theta) + 2l_4\dot{\phi}\dot{\theta} sin(\phi+\theta) + \\
l_5\dot{\phi}^2 sin(\phi+\theta+\psi) + l_5\dot{\theta}^2 sin(\phi+\theta+\psi) + l_5\dot{\psi}^2 sin(\phi+\theta+\psi) + \\
2l_5\dot{\phi}\dot{\theta} sin(\phi+\theta+\psi) + 2l_5\dot{\phi}\dot{\psi} sin(\phi+\theta+\psi) + 2l_5\dot{\theta}\dot{\psi} sin(\phi+\theta+\psi)
\end{aligned} \tag{B.12}
$$

$$
\begin{aligned}
h_8 = l_2\dot{\phi}^2 cos(\phi) + l_3\dot{\phi}^2 cos(\phi+\theta) + l_3\dot{\theta}^2 cos(\phi+\theta) + 2l_3\dot{\phi}\dot{\theta} cos(\phi+\theta) + \\
l_4\dot{\phi}^2 cos(\phi+\theta) + l_4\dot{\theta}^2 cos(\phi+\theta) + 2l_4\dot{\phi}\dot{\theta} cos(\phi+\theta) + \\
l_5\dot{\phi}^2 cos(\phi+\theta+\psi) + l_5\dot{\theta}^2 cos(\phi+\theta+\psi) + l_5\dot{\psi}^2 cos(\phi+\theta+\psi) + \\
2l_5\dot{\phi}\dot{\theta} cos(\phi+\theta+\psi) + 2l_5\dot{\phi}\dot{\psi} cos(\phi+\theta+\psi) + 2l_5\dot{\theta}\dot{\psi} cos(\phi+\theta+\psi)
\end{aligned} \tag{B.13}
$$

Forces

The force vector is formed by the external forces on the body in x and y direction and the torques around the center of mass. The only external forces besides gravity are caused by the pole. The pole forces are split up into two components, R_n and R_t. R_n points in the direction of the pole chord. The line from tip to tip of the pole. The angles λ and η are found in figure. R and η is calculated in the pole model, explained in section Pole forces.

The order of the force components is the same as the order of degrees of freedom of vector x_i. This results in the following force vector:

$$
f_i = \begin{bmatrix}
R_n cos\lambda + R_t sin\lambda \\
R_n sin\lambda + R_t cos\lambda - m_1 g \\
l_1 R_n cos(\phi+\lambda) + l_1 R_t sin(\phi+\lambda) \\
0 \\
-m_2 g \\
0 \\
0 \\
-m_3 g \\
0
\end{bmatrix} \tag{B.14}
$$

The torques generated by the torque actuators at the joints can also be seen as external forces. These torques are simply added on the right hand side of equation:

$$
y_l = \begin{bmatrix}
0 \\
0 \\
-T_1 \\
T_2 \\
T_3
\end{bmatrix} \tag{B.15}
$$

All these terms together make the equations of motion complete, resulting in the following final form:

$$
T_{i,k} M_{ij} T_{j,l} \ddot{q}_l = y_l + T_{i,k}\left(\sum f_i - M_{ij} h_j\right) \tag{B.16}
$$

Implementation in Matlab

The transformation matrix (eqn.B.7) and the convective accelerations (eqn.B.9) are determined in a separate script using a symbolic approach. The generalized coordinates (eqn.B.4) and generalized velocities are declared as symbols

in vector q and qd. The length, mass and inertia properties of the bodies are also declared as symbols. The first step is to write vector g_i (eqn.B.5) as a function of q as described above. Then, g_i is derived with respect to q, using the `jacobian` command. The convective accelerations are determined in three steps. First T_{ij} is multiplied by the generalized velocities. Then, the `jacobian` is taken with respect to q. Finally, the result is multieplied with qd, resulting in the convective accelerations.

The transformation matrix and convective accelerations are copied and paste in the function `odefun.m`. The other TMT-elements are also declared in `odefun.m`. Starting with the mass matrix, which is equal to equation B.3. The force vector is equal to equation B.14. The vector containing the control torques is equal to equationB.15.

Now, Matlab only has to fill in the variables which were declared as symbols and perform vector and matrix multiplications to create a set of equations shown in equation B.16, where the TMT multiplication results in the reduced mass matrix $\bar{M}$. The right-hand side can be seen as the extended force vector $\bar{f}$, which leaves the following equation:

$$\overline{M}\ddot{q} = \overline{f} \tag{B.17}$$

This system of equations is solved using the backslash operator, resulting in the generalized accelerations which are integrated in a numerical manner. The numerical integration is performed with the Runge-Kutta fourth order scheme which is explained in Appendix - Numerical integration with the RK4-method.

Appendix C Inertia

The inertia properties of the athlete are estimated by the method developed by Moore et al. [2009]. In his research, the inertia properties of a human together with a bike are estimated. Moore et al. [2009] simplified the human body to a tin man posture (fig. C.1). This means the upper arms, lower arms, upper legs and lower legs are represented by cylinders, the head is represented by a sphere and the torso by a cuboid.

The measurements were made as accurately as possible with basic tools but no special attention is given further to the accuracy of the calculations due to the fact that modeling the human as basic geometric shapes already introduces a large error. The circumferences were measured at the cross section where the circumference was maximum, for example around the biceps for the arms and over the nipples for the chest. The dimensions are given in table C.1.

The mass of each segment is determined as a percentage of the total body mass. The percentages per segment are based on cadaver studies. Each segment is modelled with a uniform density. So, the center of mass is located at the geometrical center of each segment. The mass of each segment is given in table C.2.

The simplified shapes and uniform density of each segment make the results less realistic. The influence of the current simplifications is partly covered in the sensitivity analysis. The inertia properties are a function of mass and shape. So, varying the length or mass of the vaulter also change the inertia properties of the vaulter and thus its final vault.

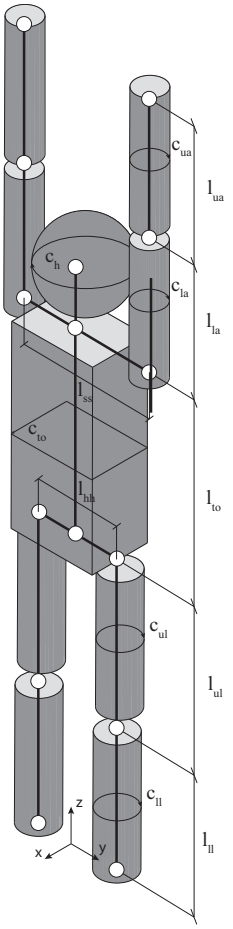

Figure C.1: The human body in 'tin man' representation [Moore et al., 2009]. The measures are found in table C.1. The figure is made by Reijne [2016]

Description	Symbol	Value	Units
circumference upper arm	c_{ua}	0.30	m
circumference lower arm	c_{la}	0.33	m
circumference head	c_h	0.58	m
circumference torso	c_{to}	0.94	m
circumference upper leg	c_{ul}	0.46	m
circumference lower leg	c_{ll}	0.38	m
length upper arm	L_{ua}	0.28	m
length lower arm	L_{la}	0.33	m
length torso	L_{to}	0.48	m
length shoulder to shoulder	L_{ss}	0.44	m
length upper leg	L_{ul}	0.46	m
length lower leg	L_{ll}	0.46	m

Table C.1: Table with measures of the tin man, given by Moore et al. [2009]. These measures are used to calculate the inertia of the vaulter.

Segment	Symbol	Equation	Value	Units
mass of vaulter's body	m_{br}	1.0 m_{br}	72	kg
upper arm	m_{ua}	0.028 m_{br}	2.02	kg
lower arm	m_{la}	0.022 m_{br}	1.58	kg
head	m_h	0.068 m_{br}	4.90	kg
torso	m_{to}	0.510 m_{br}	36.72	kg
upper leg	m_{ul}	0.100 m_{br}	7.20	kg
lower leg	m_{ll}	0.061 m_{br}	4.39	kg

Table C.2: Table with the mass per segment of the tin man, given by Moore et al. [2009]. The masses are used to calculate the inertia of the vaulter.

Calculations

Important to notice is that the optimization model is two dimensional where the model is three dimensional. There are also different global axes used. Only in this part of the appendix, the axes notation of figure C.1 is used. So, the rotations of the bodies occur only around the y-axis, according to the figure. Anywhere else in the report, the rotations occur around the z-axis.

Inertia per tin man segment

The first step to determine the inertia properties of the three segments of the vaulter, is calculating the inertia properties of each segment of the tin man. The inertia properties are calculated for rotations around the local y-axis, located at the center of mass of the segment. The inertia of the arm and leg segments is given by the inertia of a cylinder:

$$I_y = \frac{1}{12} m \left(\frac{3c^2}{4\pi^2} + l^2 \right) \tag{C.1}$$

The inertia of the head is given by the inertia of a sphere:

$$I_y = \frac{m c_h^2}{10\pi^2} \tag{C.2}$$

The inertia of the torso is given by:

$$I_y = \frac{1}{12} m \left(l_x^2 + l_z^2 \right) \tag{C.3}$$

With:

$$l_x = \frac{c_{to} - 2l_y}{\pi - 2} \tag{C.4}$$

$$l_y = L_{ss} - \frac{c_{ua}}{\pi} \tag{C.5}$$

$$l_z = L_{to} \tag{C.6}$$

Length 'l_x' estimates the thickness of the cuboid, using the chest circumference measurement and assuming that the cross section of the chest is similar to a stadium shape. Length 'l_z' is the length of the torso as given in table C.1. The resulting inertia properties per tin man segment are given in table C.3.

Tin man segments	Inertia	Units
Upper arm	0.014	kg m^2
Lower arm	0.015	kg m^2
Head	0.017	kg m^2
Torso	0.835	kg m^2
Upper leg	0.138	kg m^2
Lower leg	0.081	kg m^2

Table C.3: The inertia of the tin man segments for rotations around the local transfersal axes. The inertia is calculated according to equation C.1, equation C.2 and equation C.3

Inertia per vaulter segment

The next step is to combine the multiple tin man segments into the three vaulter segments, used in the optimization model. So, the upper arms and the lower arms are combined, the upper legs and lower legs are combined, and the head and the torso are combined to each one vaulter segment. This is done using the formula to calculate the center of mass:

$$r_{Br} = \frac{\sum m_i r_i}{m_{Br}} \tag{C.7}$$

Here, m_i is the mass of a single tin man segment, r_i is the distance from the center of mass of tin man segment i to a reference point in space. The total mass of the combined tin man segments is given by m_{br}. Finally, r_{Br} is the distance from the reference point to the center of mass of the combined tin man segments.

Then, the parallel axis theorem is used to calculate the inertia of a separate tin man segment around the combined center of mass. The inertia of the upper arm relative to the center of mass of the combined arm segments for example. The formula is given by:

$$I_i^* = I_i + m_i\left(d_z^2 + d_x^2\right) \tag{C.8}$$

Here, d_z and d_x are the distances in x- and z-direction from the combined center of mass to the center of mass of tin man segment i. The resulting I_i^* is the inertia of tin man segment i with respect to the combined center of mass. The final inertia of the resulting vaulter segment is given by:

$$\mathbf{I}_{Br} = \sum \mathbf{I}^* \tag{C.9}$$

Here, I_{Br} is the inertia of the vaulter segment around the vaulter segment's center of mass. The inertia of the arm vaulter segment, torso vaulter segment and leg vaulter segment are given in table C.4.

Combined vaulter segments	Inertia	Units
Arms	0.2235	kg m^2
Torso and head	1.3467	kg m^2
Legs	1.5941	kg m^2

Table C.4: Inertia of the combined tin man segments into vaulter segments, with respect to rotations around the transverse axis of the local centers of mass. The inertia is calculated according to equation C.7, equation C.8 and equation C.9

Inertia during the pole vault motion

The inertia of the resulting vaulter segments (the arms, legs and torso) with respect to the center of mass of the entire body, are again calculated with equation C.8, the parallel axis theorem. As the parallel axis theorem shows, the inertia of the vaulter segments depends on the distance from its local center of mass to the center of mass of the entire vaulter. Due to the movement of the segment, the position of the center of mass changes during the vaulting movement. The parallel axis theorem is therefore written as function in Matlab to calculate the inertia as a function of the position in time per combined segment.

During the development of the optimization model, the inertia properties started as a static value calculated for the initial position. With these values the vaulter could not bring his legs up, even when the torque bounds where set beyond realistic values. Figure C.2 shows four different positions of the vaulter during a vault, together with the changes in inertia over time and the previously used static values.

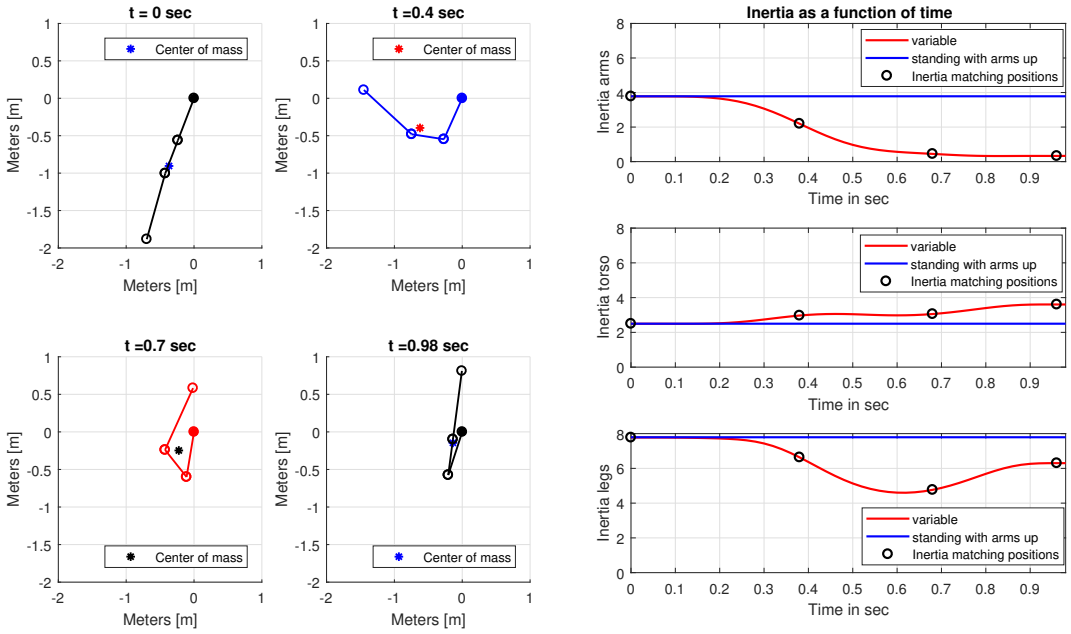

Figure C.2: Four positions are given at $t = 0.00$, $t = 0.40$, $t = 0.70$ and $t = 0.98$. The center of mass of the total body shifts as a result of the moving segments. This is illustrated in the graphs to the right where the inertia over time is shown. The upper graphs shows the inertia of the arms, the middel graph shows the inertia of the torso, the lower graph shows the inertia of the legs. The circles correspond to the positions on the left. The static values are clearly less accurate compared to the variable inertia.

The influence of a variable inertia is clearly visible. Less torque is needed to lift the legs and torso since the inertia is decreasing. It brings the optimized vault closer to reality.

Appendix D Numerical integration with the RK4-method

The numerical integration of the equations of motion (EOM) is done with the Runge-Kutta fourth order scheme. According to Boyce et al. [1992], the Runge-Kutta fourth order method is accurate enough for solving most differential equations. Besides that, the Runge-Kutta fourth order method is very straightforward to implement in Matlab.

The RK4-Scheme

The Runge-Kutta formula approximates the solution with a weighted average of four factors, k_{n1} k_{n2} k_{n3} and k_{n4}. Each factor is the output of the solved EOM, in the scheme denoted as $f(t_n, y_n)$. For every factor, t and y are varied over time interval t and $t+h$. Here, y contains the input variables q (eqn.B.4) and qd (eqn.B.6), necessary to solve the EOM. The four factors are calculated with the following input:

$$k_{n1} = f(t_n, y_n)$$
$$k_{n2} = f\left(t_n + \frac{h}{2}, y_n + \frac{h}{2}k_{n1}\right)$$
$$k_{n3} = f\left(t_n + \frac{h}{2}, y_n + \frac{h}{2}k_{n2}\right)$$
$$k_{n4} = f\left(t_n + h, y_n + hk_{n3}\right)$$

The first term, k_{n1} approximates the term at the starting point at t. The terms k_{n2} and k_{n3} approximate the slope in the middle of the interval with different input for y. The last term, k_{n4}, approximates the slope at the end of the interval, at t+h. The following weighted average over the four terms is taken:

$$y_{n+1} = y_n + h\left(\frac{k_{n1} + 2k_{n2} + 2k_{n3} + k_{n4}}{6}\right)$$

Important to notice is that the Runge-Kutta fourth order scheme solves only first order differential equations, where the EOM is a set of five second order differential equations. This is solved by introducing five new differential equations which are related to the first order time derivatives of the current five state variables:

$$\begin{bmatrix} v_x \\ v_y \\ \omega_1 \\ \omega_2 \\ \omega_3 \end{bmatrix} = \begin{bmatrix} \dot{x}_{cm_1} \\ \dot{y}_{cm_1} \\ \dot{\phi} \\ \dot{\theta} \\ \dot{\psi} \end{bmatrix}$$

The second order terms in the EOM are replaced with the first time derivative of the variables above. The angular accelerations for example, are replaced by the first order time derivative of the angular velocities $\dot{\omega}$. Now, the output of the integrated set of differential equations results in the input needed for the next integration step.

Implementation in Matlab

The Runge-Kutta scheme is implemented as a separate function in Matlab. The input for the `rk4step.m` is the function containing the equations of motion `odefun.m`, the input for the equations of motion `INP_ODE`, time t, step size h, the generalized positions and generalized velocities at t and the input vectors for the three torque functions. The four terms k_{n1}, k_{n2}, k_{n3} and k_{n4} are calculated with the function `feval`. For each term, t and y are changed according to the scheme. As explained in the appendix script, the output of `odefun` depends on whether there is a solution found in the pole model. If this is not the case, `odefun` returns a vector with only zero's. The function

`rk4step` checks if there are terms which are only zero. In that case it returns a vector with only zeros to either `objective.m` or `nonlcon.m`. The vector with zeros forces the functions to stop the motion. If the pole model did find a solution, the weighted average is taken over the four terms, resulting in the positions q and velocities $\dot{q}$ at time $= t + h$.